Icarus 203 (2009) 644–662

Contents lists available at ScienceDirect

Icarus

journal homepage: www.elsevier.com/locate/icarus

Building the terrestrial planets: Constrained accretion in the inner Solar System

Sean N. Raymond [a,*], David P. O'Brien [b], Alessandro Morbidelli [c], Nathan A. Kaib [d]

[a] Center for Astrophysics and Space Astronomy, University of Colorado, UCB 389, Boulder, CO 80309-0389, USA
[b] Planetary Science Institute, Tucson, AZ, USA
[c] Observatoire de la Côte d'Azur, Boulevard de l'Observatoire, BP 4229, 06304 Nice Cedex 4, France
[d] Department of Astronomy, University of Washington, Seattle, WA 98195, USA

ARTICLE INFO

Article history:
Received 22 January 2009
Revised 14 April 2009
Accepted 17 May 2009
Available online 2 June 2009

Keywords:
Terrestrial planets
Planetary formation
Accretion
Origin
Solar System

ABSTRACT

To date, no accretion model has succeeded in reproducing all observed constraints in the inner Solar System. These constraints include: (1) the orbits, in particular the small eccentricities, and (2) the masses of the terrestrial planets – Mars' relatively small mass in particular has not been adequately reproduced in previous simulations; (3) the formation timescales of Earth and Mars, as interpreted from Hf/W isotopes; (4) the bulk structure of the asteroid belt, in particular the lack of an imprint of planetary embryo-sized objects; and (5) Earth's relatively large water content, assuming that it was delivered in the form of water-rich primitive asteroidal material. Here we present results of 40 high-resolution ($N = 1000$–2000) dynamical simulations of late-stage planetary accretion with the goal of reproducing these constraints, although neglecting the planet Mercury. We assume that Jupiter and Saturn are fully-formed at the start of each simulation, and test orbital configurations that are both consistent with and contrary to the "Nice model". We find that a configuration with Jupiter and Saturn on circular orbits forms low-eccentricity terrestrial planets and a water-rich Earth on the correct timescale, but Mars' mass is too large by a factor of 5–10 and embryos are often stranded in the asteroid belt. A configuration with Jupiter and Saturn in their current locations but with slightly higher initial eccentricities ($e = 0.07$–0.1) produces a small Mars, an embryo-free asteroid belt, and a reasonable Earth analog but rarely allows water delivery to Earth. None of the configurations we tested reproduced all the observed constraints. Our simulations leave us with a problem: we can reasonably satisfy the observed constraints (except for Earth's water) with a configuration of Jupiter and Saturn that is at best marginally consistent with models of the outer Solar System, as it does not allow for any outer planet migration after a few Myr. Alternately, giant planet configurations which are consistent with the Nice model fail to reproduce Mars' small size.

1. Introduction

It is commonly accepted that rocky planets form by the process of collisional agglomeration of smaller bodies (for recent reviews, see Chambers, 2004; Nagasawa et al., 2007 or Raymond, 2008). This process starts from micron-sized dust grains in young circumstellar disks, and the current paradigm proceeds as follows. Grains settle to a thin disk midplane on a $\sim 10^4$ year timescale (Weidenschilling, 1980), and grow quickly via sticky collisions until they reach cm- or m-sizes (Dullemond and Dominik, 2004). The time for m-sized bodies to spiral in to the star is very short (~100 years) such that this size range constitutes a barrier to further growth (Weidenschilling, 1977a). This barrier may be crossed by rapid accretion (Weidenschilling and Cuzzi, 1993; Benz, 2000) or by local gravitational instability (Goldreich and Ward, 1973; Youdin and Shu, 2002), which can be triggered by turbulent concentration (Johansen et al., 2007; Cuzzi et al., 2008). Larger bodies (100 m to 100 km in size), which are more weakly coupled to the gaseous disk, are called planetesimals. Runaway growth of the largest planetesimals may occur while the velocity dispersion is small because of strong gravitational focusing such that $dM/dt \sim M^{4/3}$ (Safronov, 1969; Greenberg et al., 1978. However, viscous stirring by the large bodies increases the velocity dispersion of planetesimals, thereby reducing the growth rate to a roughly geometrical regime, where $dM/dt \sim M^{2/3}$ (Ida and Makino, 1993). Dynamical friction acts on the oligarchs, maintaining small eccentricities (Ida and Makino, 1992; Kokubo and Ida, 1998). The building blocks of the terrestrial planets, approximately Moon-sized planetary embryos, form in 10^5–10^6 years with a characteristic spacing of 5–10 mutual Hill radii (Wetherill and Stewart, 1993; Weidenschilling et al., 1997; Kokubo and Ida, 2000, 2002). Giant collisions between planetary embryos begin to occur when the local density of planetesimals and embryos is comparable (Wetherill, 1985; Kenyon and Bromley, 2006). During late-stage accretion, embryo–planetesimal and embryo–embryo impacts are common and the feeding zones

* Corresponding author.
E-mail address: sean.raymond@colorado.edu (S.N. Raymond).

0019-1035/$ - see front matter © 2009 Elsevier Inc. All rights reserved.
doi:10.1016/j.icarus.2009.05.016

of terrestrial planets can span several AU in width (Raymond et al., 2006). Late-stage accretion lasts for $\sim 10^8$ years and sets the final bulk architecture of the system as well as the composition of the terrestrial planets (e.g., Wetherill, 1996).

Past simulations of late-stage accretion have succeeded in reproducing several aspects of the Solar System's terrestrial planets. Using only 20–165 particles, Agnor et al. (1999) and Chambers (2001) roughly reproduced the approximate masses and semimajor axes of Mercury, Venus, Earth and Mars. Thommes et al. (2008) also reproduced the rough mass distribution of the inner Solar System by invoking sweeping secular resonances during the depletion of the Solar Nebula. By taking dynamical friction from remnant planetesimals into account, O'Brien et al. (2006) and Morishima et al. (2008) reproduced the very low eccentricities of the terrestrial planets. Several groups have succeeded in delivering water to Earth from hydrated asteroidal material, following the model of Morbidelli et al. (2000), see also Raymond et al., 2004, 2006, 2007 and O'Brien et al., 2006.

Despite these achievements, no previous study has adequately reproduced all aspects of the inner Solar System. Indeed, as pointed out by Wetherill (1991), Mars' small size remains the most difficult constraint to reproduce (also discussed in Chambers, 2001). Agnor et al. (1999), Chambers (2001) and Morishima et al. (2008) succeeded in reproducing Mars' small size only because their simulations started from an annulus of material with a fixed width (see also Kominami and Ida, 2002). In most cases this annulus extended from 0.5 to 1.5 AU, such that a small planet could form at the outer edge of the initial disk because of spreading. However, no such edge is thought to have existed in the Solar Nebula, so that the assumption that the planetesimal and embryo population extended only to 1.5 AU is not justified. Chambers (2001) managed to place Mercury within a planetary mass distribution but only by adopting an ad hoc inner disk profile. Thommes et al. (2008) formed a small Mars but the orbits they assumed for Jupiter and Saturn are inconsistent with any significant late, planetesimal-driven migration of the giant planets (discussed at length in Section 6.2 below). In fact, the scenario of Thommes et al. (2008) is incompatible with the two currently viable theories for the late heavy bombardment (Tera et al., 1974) because these require either a more compact configuration of Jupiter and Saturn (Gomes et al., 2005) or the formation of a small, sub-Mars-sized planet at ~2 AU (Chambers, 2007).

Terrestrial accretion lasts for $\sim 10^8$ years, far longer than the few Myr lifetimes of the gaseous component of protoplanetary disks (Haisch et al., 2001; Briceño et al., 2001; Pascucci et al., 2006). Thus, gas giant planets must be fully-formed during late-stage accretion and can therefore strongly affect terrestrial bodies, especially if the giant planets' orbits are eccentric (Wetherill, 1996; Chambers and Cassen, 2002; Levison and Agnor, 2003; Raymond et al., 2004; O'Brien et al., 2006). Given that substantial orbital migration of the Solar System's giant planets has been proposed to explain the structure of the Kuiper Belt (Fernandez and Ip, 1984; Malhotra, 1995) and the origin of the late heavy bombardment (Strom et al., 2005; Gomes et al., 2005), the orbits of Jupiter and Saturn at early times are unclear. Indeed, a range of Jupiter–Saturn configurations could yield the current Solar System. Thus, if any particular configuration were especially adept at reproducing the terrestrial planets, it would provide strong circumstantial evidence in favor of that configuration.

In this paper we attempt to reproduce the inner Solar System with a suite of high-resolution (N = 1000–2000) dynamical simulations of late-stage accretion. We only vary one parameter of consequence: the configuration of Jupiter and Saturn at early times. We quantify five relevant constraints that we use to test our models in Section 2. In Section 3, we outline our choices of initial conditions and numerical methods. In Section 4 we explore the case of two contrasting simulations that each reproduce certain constraints. We present results and analysis of all simulations in Section 5. We discuss these results and present our conclusions in Section 6.

2. Inner solar system constraints

We consider five broad attributes which we attempt to reproduce statistically with accretion simulations. Other observations and measurements exist for inner Solar System bodies, but we are limiting ourselves to relatively broad and well-understood characteristics. These constraints are described below in order from strongest to weakest. Weaker constraints rely on models or data that are subject to interpretation, while strong constraints are directly observed. We use several quantities to compare our simulations with the Solar System's terrestrial planets. These include statistical measures that were introduced by Chambers (2001).

1. The masses and the mass distribution of the terrestrial planets. As mentioned above, the mass distribution of the terrestrial planets, and in particular the small masses of Mercury and Mars, have not been adequately reproduced in the context of the entire Solar System and its history. In this paper we do not attempt to reproduce Mercury because its small size and large iron content may be the result of a mantle-stripping impact (Benz et al., 1988) or interesting composition-sorting gaseous effects (Weidenschilling, 1978). However, for the case of Mars, with its more distant orbit, these effects are less likely to be a factor, and it should be reproducible in the context of our simulations. In addition, the distribution of mass in the inner Solar System is interesting because the majority is concentrated between the orbits of Venus and Earth. We therefore use two statistical measures for this constraint:

- The number of planets formed N_p. We take N_p to represent objects that contain at least one planetary embryo, that have semimajor axes $a < 2$ AU, and that are on long-term stable orbits. It is only for these planets that we apply our other measures.
- A radial mass concentration statistic *RMC* (called S_c in Chambers, 2001):

$$RMC = max\left(\frac{\sum M_j}{\sum M_j[log_{10}(a/a_j)]^2}\right), \quad (1)$$

where M_j and a_j are the masses and semimajor axes of each planet. The function in brackets is calculated for a throughout the terrestrial planet zone, and RMC is the maximum of that function. This quantity represents the degree to which mass is concentrated in a small radial annulus: RMC remains small for a system of many equal-mass planets but RMC is large for systems with few planets and with most of the mass in one or two planets. For a one planet system, the *RMC* value is infinite. The *RMC* of the Solar System's terrestrial planets is 89.9 (see Table 2).

2. The orbits of the terrestrial planets. The terrestrial planets maintain very small orbital eccentricities and inclinations over long timescales. Earth and Venus' time-averaged eccentricities are only about 0.03 (e.g., Quinn et al., 1991). Recent simulations with $N \geqslant 1000$ particles have succeeded in reproducing these small eccentricities for the first time (O'Brien et al., 2006). We quantify the orbital excitation of the terrestrial planets using the normalized angular momentum deficit *AMD* (Laskar, 1997). This measures the difference in angular momentum of a set of orbits from coplanar, circular orbits:

$$AMD = \frac{\sum_j m_j\sqrt{a_j}\left(1 - cos(i_j)\sqrt{1-e_j^2}\right)}{\sum_j m_j\sqrt{a_j}}, \quad (2)$$

where a_j, e_j, i_j, and m_j refer to planet j's semimajor axis, eccentricity, inclination with respect to a fiducial plane, and mass. The *AMD* of the Solar System's terrestrial planets is 0.0018 (see Table 2).

3. The formation timescales of Earth and Mars. Recent interpretation of Hf/W measurements suggest that the last core-formation event on Earth occurred at roughly 50–150 Myr (Touboul et al., 2007)[1] This event is thought to be the Moon-forming impact (Benz et al., 1986; Canup and Asphaug, 2001). Mars' formation time from Hf/W isotopes appears to be significantly shorter, about 1–10 Myr (Nimmo and Kleine, 2007).

4. The large-scale structure of the asteroid belt. The asteroid belt shows a clear division between inner, S-types and more distant C-types (e.g., Gradie and Tedesco, 1982). In addition, there are no large gaps in the main belt except those caused by specific mean motion or secular resonances. If a planetary embryo above a critical mass were stranded in the asteroid belt for a long period of time, it would disrupt both of these observed characteristics by planetesimal scattering (O'Brien et al., in preparation). This constraint puts an upper limit of a few lunar masses ($\sim 0.05\ M_\oplus$) on the mass of an object that can survive in the asteroid belt after terrestrial planet formation. If an embryo did end up in the main belt, it could have been subsequently removed during the late heavy bombardment (Gomes et al., 2005; Strom et al., 2005), but the embryo's dynamical imprint on the asteroid belt would have remained.[2] We note that the asteroid belt is thought have been depleted by a factor of $\sim 10^4$ in mass over the lifetime of the Solar System. This depletion is best explained by scattering of planetesimals by planetary embryos in the primordial belt (Wetherill, 1992; Chambers and Wetherill, 2001; Petit et al., 2001; O'Brien et al., 2007), although other models do exist (e.g., Lecar and Franklin, 1997; Nagasawa et al., 2000). Scattering among embryos often places one body in an unstable mean motion resonances with Jupiter, leading to their rapid removal from the belt. This scattering also leads to some radial mixing, consistent with the observation that the different asteroid taxonomic types are not confined to narrow zones, but are spread somewhat in overlapping but still distinct regions (Gradie and Tedesco, 1982). Embryos as small as the Moon are able to provide the necessary excitation (Chambers and Wetherill, 2001). Most of the embryos are removed on a timescale of $\sim$10 Myr. However, if one or more stray embryos with too large of a mass remain in the belt for much longer than this, they will lead to excessive radial mixing, inconsistent with the observed distribution of different asteroid taxonomic types. Fig. 1 shows the effect of a Mars-mass embryo trapped at 2.5 AU on 100 Myr of evolution of 1000 asteroids in the main belt (2–3.5 AU), which are assumed to be massless. Two features from Fig. 1 are inconsistent with the observed main belt: the excess radial mixing and the gap created in the vicinity of the embryo. More massive or more eccentric asteroidal embryos can be significantly more disruptive than the case from Fig. 1, especially if their eccentricity is strongly forced by secular perturbations from Jupiter and Saturn (O'Brien et al., in preparation). In addition, the simulation from Fig. 1 was only run for 100 Myr, roughly 500 Myr shorter than the relevant timescale, i.e., the time between the completion of terrestrial accretion ($\sim$100 Myr) and the time of the late heavy bombardment (600–700 Myr). Thus, the constraint we place on our accretion simulations is that no embryos larger than $0.05\ M_\oplus$ can survive in the main belt past the end of terrestrial planet growth, or in our case 2×10^8 years.

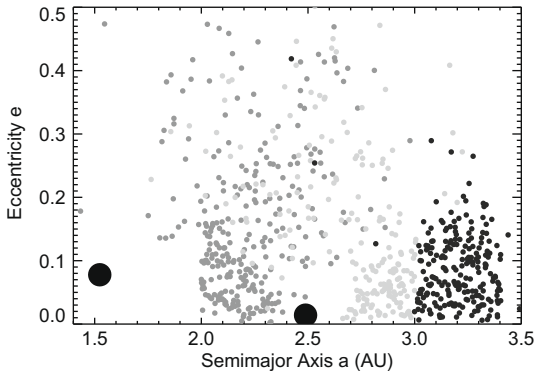

Fig. 1. The effect of a Mars-sized planetary embryo on the structure of the asteroid belt. Shown are the surviving (massless) asteroidal bodies, whose orbits were integrated for 100 Myr under the influence of Jupiter and Saturn (not shown), Mars and a Mars-mass planetary embryo stranded in the asteroid belt at 2.49 AU. Asteroids are color-coded according to their starting semimajor axes: grey (2–2.5 AU), light grey (2.5–3 AU), and black (3–3.5 AU).

5. Earth's water content. One prominent model suggests that primitive asteroidal material was the source of the bulk of Earth's water (Morbidelli et al., 2000; see also Raymond et al., 2007). This model explains why the D/H ratio of Earth's water matches that of carbonaceous chondrites (Robert and Epstein, 1982; Kerridge, 1985), and links Earth's water to the depletion of the primitive asteroid belt. Note that other models exist which propose that Earth's water came from comets (Delsemme, 1992; Owen and Bar-Nun, 1995), from oxidation of a primitive, H-rich atmosphere (Ikoma and Genda, 2006), from adsorption of water onto small grains at 1 AU (Muralidharan et al., 2008), or from other sources – see Morbidelli et al. (2000) for a discussion of some of these models. However, it is our opinion that the asteroidal water model of Morbidelli et al. (2000) is the most likely source of Earth's water. In fact, water vapor from sublimation of in-spiraling icy bodies has been detected interior to 1 AU in the protoplanetary disk around the young star MWC480 (Eisner, 2007); this may be an observation of asteroidal (or in this case potentially cometary) water delivery in action.

3. Methods

Our simulations are designed to start at the beginning of late-stage accretion, after Jupiter and Saturn are fully-formed and the nebular gas has dissipated. This is probably 1–3 Myr after "time zero", and we base our initial conditions on models of the formation of planetary embryos (e.g., Kokubo and Ida, 2000). We start with a disk of planetary embryos and planetesimals, plus Jupiter and Saturn. Our simulations are comparable to the highest-resolution cases in the literature, containing 85–90 planetary embryos and 1000–2000 planetesimals.[3]

3.1. Configuration of Jupiter and Saturn

The resonant structure of the Kuiper Belt appears to require a significant outward migration of Neptune (Fernandez and Ip, 1984; Malhotra, 1995; Gomes, 2003; Levison and Morbidelli,

[1] Touboul et al.'s (2007) core-formation age is roughly a factor of two longer than previous estimates (Kleine et al., 2002; Yin et al., 2002). It is important to note that Hf/W measurements of Earth samples are somewhat uncertain given the unknown amount of core/mantle equilibration during giant impacts (Halliday, 2004; Nimmo and Agnor, 2006). However, the samples from Touboul et al. (2007) are lunar in origin and therefore circumvent the issue of equilibration.

[2] It is important to note that the late heavy bombardment was a purely dynamical event, as shown by the difference between crater size distributions on surfaces older vs. younger than 3.8 Gyr (Strom et al., 2005).

[3] The highest-resolution published late-stage accretion simulations to date had N = 2000–3000 (Raymond et al., 2006; Morishima et al., 2008).

2003). This outward migration occurred because of the back-reaction from planetesimal scattering, which causes the orbits of Saturn, Uranus and Neptune to expand and the orbit of Jupiter to contract (Fernandez and Ip, 1984). In addition, the "Nice model" of giant planet evolution, which explains several observed characteristics of the Solar System, proposes that Jupiter and Saturn formed interior to their mutual 2:1 mean motion resonance, perhaps in fact in the 3:2 resonance and migrated apart (Tsiganis et al., 2005; Gomes et al., 2005; Morbidelli et al., 2005, 2007). Thus, Jupiter and Saturn may very well have been in a more compact configuration at early times.

We tested a range of configurations for Jupiter and Saturn, although we did not perform an exhaustive search given the large computational expense of each simulation. However, to account for stochastic variations in outcome we performed four simulations for each giant planet configuration. The configurations we tested were:

- CJS ("Circular Jupiter and Saturn"). These are the initial conditions for the Nice model, as in Tsiganis et al. (2005) and also used in O'Brien et al. (2006). Jupiter and Saturn were placed on circular orbits with semimajor axes of 5.45 and 8.18 AU and a mutual inclination of 0.5°. We note that even though Jupiter and Saturn begin with zero eccentricities, they induce small, non-zero eccentricities in each others' orbits.
- CJSECC ("CJS with ECCentric orbits"). Jupiter and Saturn were placed at their CJS semimajor axes of 5.45 and 8.18 AU with $e_J = 0.02$ and $e_S = 0.03$ and a mutual inclination of 0.5°.
- EJS ("Eccentric Jupiter and Saturn"). Jupiter and Saturn were placed on approximately their current orbits: $a_J = 5.25$ AU, $e_J = 0.05$, $a_S = 9.54$ AU, and $e_S = 0.06$, with a mutual inclination of 1.5°.
- EEJS ("Extra Eccentric Jupiter and Saturn"). Jupiter and Saturn were placed at their current semimajor axes but with higher orbital eccentricities: $a_J = 5.25$ AU, $a_S = 9.54$ AU, and $e_J = e_S = 0.1$, with a mutual inclination of 1.5°. These cases proved to be interesting, so we ran eight cases in addition to the original four. The next four cases (referred to as EEJS 5-8) had the same configuration of Jupiter and Saturn but 2000 planetesimals rather than 1000. The final four cases (EEJS 9-12) also had 2000 planetesimals but had $e_J = 0.07$ and $e_S = 0.08$.
- JSRES ("Jupiter and Saturn in RESonance"). Jupiter and Saturn were placed in their mutual 3:2 mean motion resonance, following directly from simulations of their evolution in the gaseous Solar Nebula (Morbidelli et al., 2007): $a_J = 5.43$ AU, $a_S = 7.30$ AU, $e_J = 0.005$, and $e_S = 0.01$, with a mutual inclination of 0.2°.
- JSRESECC ("Jupiter and Saturn in RESonance on ECCentric orbits"). As for JSRES but with $e_J = e_S = 0.03$.

The EJS and EEJS simulations assume that Jupiter and Saturn did not undergo any migration. The EEJS simulations are more self-consistent than the EJS simulations, because scattering of remnant planetesimals and embryos tends to decrease the eccentricities and semimajor axes of Jupiter and Saturn (e.g., Chambers, 2001). Thus, to end up on their current orbits, Jupiter and Saturn would have had to form on more eccentric and slightly more distant orbits. The CJS, JSRES and JSRESECC simulations all follow from the Nice model and assume that Jupiter and Saturn's orbits changed significantly after their formation, with Saturn migrating outward and Jupiter inward (Tsiganis et al., 2005). If migration of the giant planets is really associated with the late heavy bombardment (Gomes et al., 2005; Strom et al., 2005), then at least most of the migration of Jupiter and Saturn must have occurred late, well after the completion of the terrestrial planet formation process.

3.2. Properties of the protoplanetary disk

For all of our simulations, the disk of solids extended from 0.5 to 4.5 AU and contained populations of planetary embryos and planetesimals. For most cases, we assumed that the disk's surface density in solids Σ followed a simple radial power-law distribution:

$$\Sigma(r) = \Sigma_1 \left(\frac{r}{1\mathrm{AU}}\right)^{-x}. \quad (3)$$

For the minimum-mass Solar Nebula (MMSN) model, $\Sigma_1 \approx 6$–7 g cm^{-2} and $x = 3/2$ (Weidenschilling, 1977b; Hayashi, 1981). For most of our simulations we assumed $x = 3/2$ but we also performed some cases with $x = 1$ for the CJS and EJS giant planet configuration. Cases with $x = 1$ are labeled by the x value; for example, the EJS15 simulations have $x = 3/2$ and the EJS1 simulations have $x = 1$ (see Table 2). For each case, we calibrated our disks to contain a total of 5 $M_\oplus$ in solids between 0.5 and 4.5 AU, divided equally between the planetesimal and embryo components.

Fig. 2 shows a sample set of initial conditions. We assumed that embryos are spaced by $\Delta = 3$–6 mutual Hill radii R_H, where $R_H = 0.5(r_1 + r_2)\,[(M_1 + M_2)/3M_\odot]^{1/3}$, where a_1 and M_1 are the radial distance and mass of embryo 1. The embryo mass therefore scales with orbital distance as $M \sim r^{3/2\,(2-x)}\Delta^{3/2}$ (Kokubo and Ida, 2002; Raymond et al., 2005). The disks contained 85–90 embryos with masses between 0.005 and 0.1 $M_\oplus$. In Mars' vicinity the typical embryo mass was roughly 1/6–1/3 of a Mars mass. Planetesimals were laid out as $N_p \sim r^{x+1}$ to follow the annular mass, and had masses of 0.0025 $M_\oplus$. Embryos and planetesimals were given randomly-chosen starting eccentricities of less than 0.02 and inclinations of less than 0.5°. In a few EEJS cases we performed additional simulations with 2000 planetesimals, which followed the same distribution but had correspondingly smaller masses.

We assume that there existed a radial compositional gradient for rocky bodies in the Solar Nebula. This gradient was presumably imprinted on planetesimals by the local temperature during their formation (e.g., Boss, 1998), although heating by short-lived radionuclides such as ^{26}Al may have played a role (Grimm and McSween, 1993). We assume the same water distribution as in Raymond et al. (2004, 2006), using data for primitive meteorites from Abe et al. (2000). The "water mass fraction", *WMF*, i.e. the water content by mass, varies with radial distance r as

$$WMF = \begin{cases} 10^{-5}, & r < 2\mathrm{AU} \\ 10^{-3}, & 2\mathrm{AU} < r < 2.5\mathrm{AU} \\ 5\%, & r > 2.5\mathrm{AU} \end{cases} \quad (4)$$

This water distribution is imprinted on planetesimals and embryos at the start of each simulation. During accretion the water

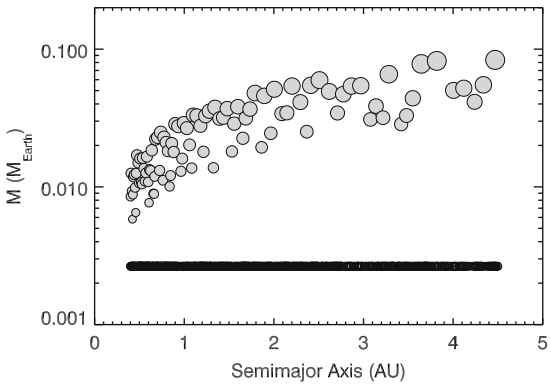

Fig. 2. Sample initial conditions for a disk with $\Sigma \sim r^{-3/2}$ containing 97 planetary embryos and 1000 planetesimals. Embryos are shown in gray with their sizes proportional to their mass$^{(1/3)}$ (but not to scale on the x axis).

content of each body is calculated by a simple mass balance of all the accreted bodies. We do not take into account water loss during giant impacts (Genda and Abe, 2005; Canup and Pierazzo, 2006) or via hydrodynamic escape (Matsui and Abe, 1986; Kasting, 1988).

3.3. Numerical method

Each simulation was integrated for at least 200 Myr using the hybrid symplectic integrator `Mercury` (Chambers, 1999). We used a 6-day timestep for all integrations; numerical tests show that this is adequate to resolve the innermost orbits in our simulations and to avoid any substantial error buildup (see Rauch and Holman, 1999). Collisions are treated as inelastic mergers, and we assumed physical densities of 3 g cm^{-3} for all embryos and planetesimals. Simulations were run on individual machines in a distributed computing environment, and required 2–4 months per simulation. The Sun's radius was artificially increased to 0.1 AU to avoid numerical error for small-perihelion orbits.

For each Jupiter–Saturn-disk configuration we performed four different simulations to account for the stochastic nature of accretion (e.g., Chambers and Wetherill, 1998). These four cases varied in terms of the random number used to initialize our disk code, resulting in differences in the detailed initial distributions of embryos and planetesimals.

Embryo particles interacted gravitationally with all other bodies but planetesimal particles did not interact with each other. This approximation was made to reduce the run time needed per simulation which is already considerable (see Raymond et al., 2006 for a discussion of this issue). The run time τ scales with the number of embryos N_e and the number of planetesimals, N_p, roughly as $\tau \sim N_e^2 + 2N_eN_p$. The non-interaction of planetesimals eliminates an additional N_p^2 term. Note that τ refers to the computing time needed for a given timestep. The total runtime is τ integrated over all timesteps for all surviving particles. Thus, a key element in the actual runtime of a simulation is the mean particle lifetime. Configurations with strong external perturbations (e.g., eccentric giant planets) tend to run faster because the mean particle lifetime is usually shorter than for configurations with weak external perturbations.

4. Two contrasting examples

We illustrate the variations between different cases using two simulations with different configurations of Jupiter and Saturn: one case from the JSRES batch and one from EEJS (simulations JSRES-4 and EEJS-3 in Table 2). Each simulation matched some of our constraints but neither matched all of them. Figs. 3 and 4 show snapshots in the evolution of the two simulations. Properties of the planets that formed in each case are listed in Table 1. We note that these are individual simulations, and that there exists substantial variability in outcome between simulations even for the same giant planet configuration. We discuss the outcomes of all simulations in Section 5.

In the JSRES simulation (Fig. 3), eccentricities are excited in the inner disk by interactions between embryos and planetesimals. In the outer disk, eccentricities are excited by specific mean motion resonances (MMRs) with Jupiter and Saturn: the 3:1, 2:1 and 3:2 MMRs are clearly visible. Eccentric embryos perturb nearby bodies and act to spread out the resonant excitation on a Myr timescale. A stage of chaotic growth lasts for ~100 Myr. During this time, there is substantial mixing of objects between radial zones, the inner system is cleared of small bodies, and four water-rich planets are formed inside 2 AU with masses between 0.36 and 0.95 $M_\oplus$ (see Table 1).

In the EEJS simulation (Fig. 4), the inner and outer portions of the disk are quickly divided by a strong secular resonance near 2 AU (ν_6). The evolution of the inner disk proceeds in similar fashion to the JSRES simulation, although eccentricities are higher because of excitation by another secular resonance at 0.7 AU (ν_5). The asteroid belt region was cleared more quickly than for the JSRES case due to stronger secular and resonant perturbations. The stage of chaotic growth also lasts about 10^8 years but with less mixing between radial zones. At the end of the simulation, three mainly dry planets have formed within 2 AU. The outermost planet lies at 1.63 AU and is a good Mars analog.

Fig. 5 (top panels) shows the masses of the planets over the 200 Myr span of the simulation for the two simulations. Planetary growth is a combination of relatively smooth accumulation from a large number of planetesimals and punctuated accretion from a small number of giant impacts with other embryos. In general, embryo–embryo collisions increase in magnitude in time simply because all embryos are growing. This is particularly clear for the case of the innermost planet (0.59 AU) in the JSRES simulation which was hit by a 0.41 $M_\oplus$ embryo at 94.8 Myr while the planet was only 0.48 $M_\oplus$.

The timescale for the last giant impact on the JSRES planets was 43–160 Myr, and 0.17–82 Myr for the EEJS planets. The Earth analog (i.e., the planet closest to 1 AU) in each simulation fell slightly out of the 50–150 Myr window for the last giant impact on Earth (Touboul et al., 2007), but on different sides. The JSRES Earth analog's last giant impact was slightly too late (160 Myr) while the EEJS Earth analog's was too early (35.6 Myr). The Mars analog in the JSRES simulation (at 1.42 AU) has a mass that is roughly eight times too large and a formation timescale that is far too long (124 Myr as compared with the Hf/W isotopic age of 1–10 Myr; Nimmo and Kleine, 2007). In contrast, the EEJS simulation produced an excellent Mars analog that is actually somewhat smaller than Mars (0.06 $M_\oplus$ vs. 0.11 $M_\oplus$) and whose only giant impact occurred 168,000 years into the simulation. Given that the "time zero" for our simulations is probably 1–3 Myr after the formation of the Solar Nebula, this is consistent with isotopic measurements. It is interesting to note that the last giant impact on the innermost planet in each simulation occurred quite late, at ~10^8 years (see Table 1). The reason for the late impact was different for the two simulations. For the JSRES simulation the last giant impactor originated in the asteroid belt, where the timescale for close encounters and scattering is longer than the inner system. For the EEJS simulation, the last giant impactor originated at 1.2 AU but had its inclination increased by a short time spent in the vicinity of the ν_6 secular resonance, thereby prolonging its dynamical lifetime in the inner system. These late giant impacts on close-in planets contrast with the nominal view of accretion occurring fastest in the inner regions of the disk, especially given the much shorter accretion timescales for the Earth and Mars analogs in the EEJS simulation.

The feeding zones of the planets from the JSRES and EEJS simulations are shown in the bottom panels of Fig. 5. Feeding zones were calculated as the fraction of material incorporated into each planet that originated in each 0.45 AU-wide radial bin. The feeding zones of all planets overlap in each simulation, although the width of individual feeding zones vary.[4] In the JSRES simulation each of the four planets accreted material from a radial width of more than 3 AU. Given that the source of water lies beyond 2–2.5 AU, this explains the large water abundance in the JSRES planets. The Earth analog's feeding zone is exceedingly wide and is unusual in that its accretion seed actually started the simulation in the outer asteroid belt, at 4.3 AU.[5] The Earth analog's water content was therefore very large, roughly 30 times the

[4] Terrestrial feeding zones are not static, but actually widen and move outward in time (Raymond et al., 2006).

[5] A planet's accretion seed is simply the object that was the larger in each of its collisions. The planet retains the name of this object.

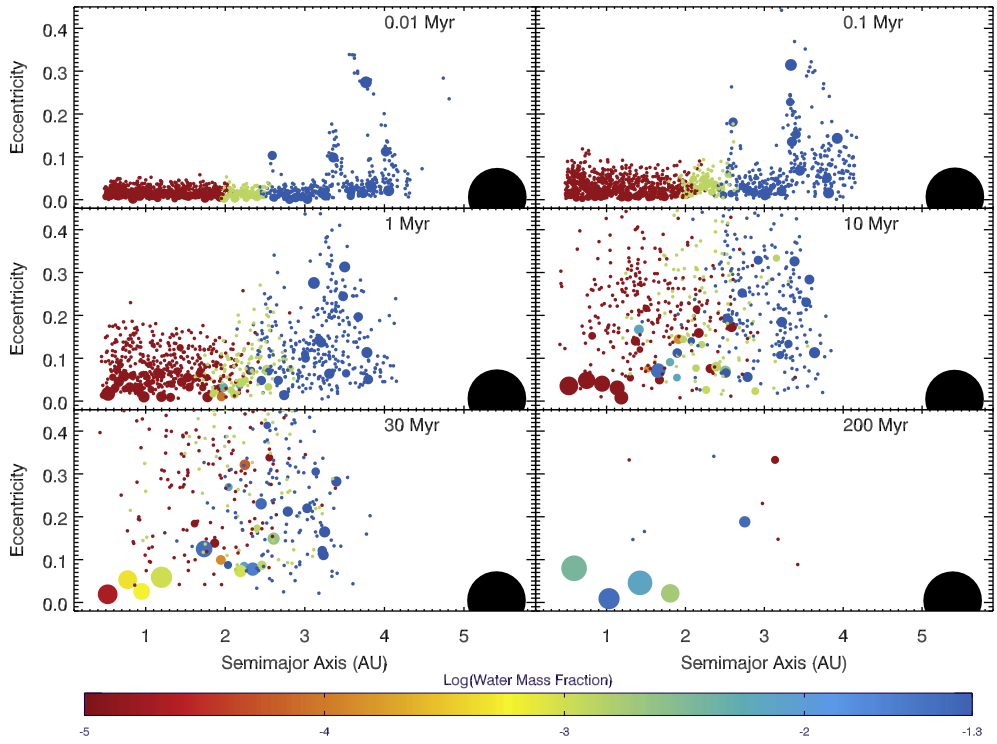

Fig. 3. Snapshots in time from a simulation with Jupiter and Saturn in 3:2 mean motion resonance (JSRES). The size of each body is proportional to its mass$^{(1/3)}$ (but is not to scale on the x axis). The color of each body corresponds to its water content by mass, from red (dry) to blue (5% water). Jupiter is shown as the large black dot; Saturn is not shown.

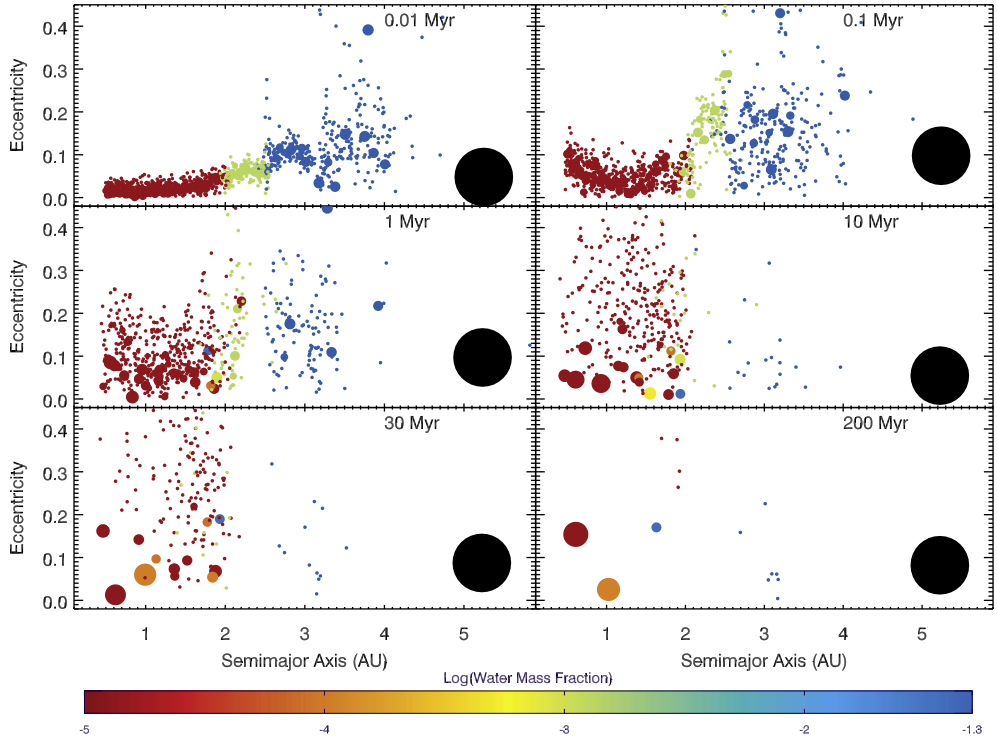

Fig. 4. Evolution of a simulation with Jupiter and Saturn starting at their current semimajor axes but with eccentricities of 0.1 (EEJS). Formatted as in Fig 3.

Earth's current water content without accounting for any water loss (the Earth's *WMF* is $\sim 10^{-3}$; Lécuyer et al., 1998). In contrast, the three planets from the EEJS simulations each had feeding zones of less than 1.7 AU in width. Very little material from exterior to 2 AU was incorporated into the EEJS planets, with the notable exception of one embryo that originated at 2.64 AU and was the accretion seed of the Mars analog. Thus, the Earth and Venus analogs are very dry, but the Mars analog is very water-rich.

Table 1
Planets that formed in the JSRES and EEJS example simulations.

Planet	a (AU)	e[a]	i (deg)	Mass ($M_\oplus$)	$WMF_\oplus$	Last giant impact (Myr)
JSRES-a	0.59	0.08	1.7	0.95	2.77×10^{-3}	113.5
JSRES-b	1.03	0.03	2.8	0.54	2.87×10^{-2}	160.0
JSRES-c	1.42	0.03	2.5	0.85	5.48×10^{-3}	124.1
JSRES-d	1.81	0.02	4.7	0.36	1.42×10^{-3}	42.9
EEJS-a	0.61	0.08	3.3	0.90	1×10^{-5}	82.2
EEJS-b	1.02	0.05	3.2	0.70	7.14×10^{-5}	35.6
EEJS-c	1.63	0.16	9.0	0.06	3.08×10^{-2}	0.168

[a] Orbital values (a, e, i) are averaged over the last 1 Myr of each simulation.

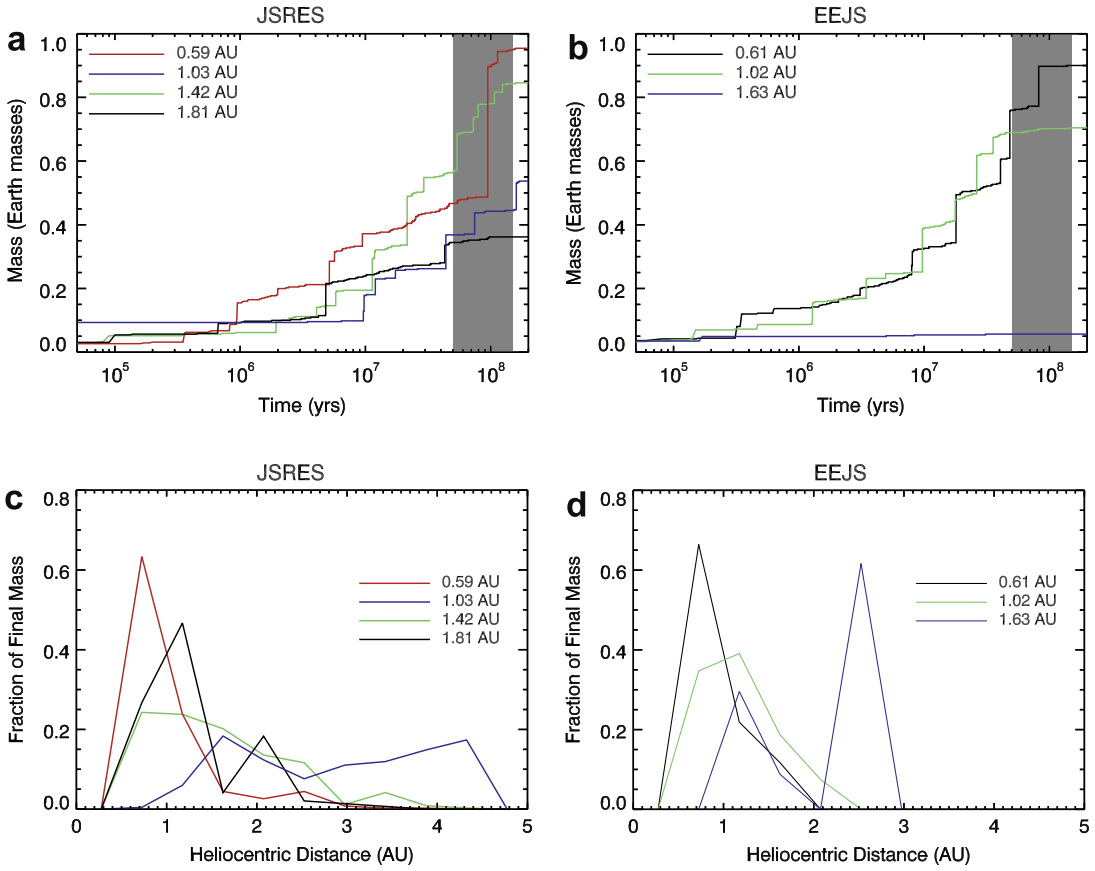

Fig. 5. Growth and feeding zones for the planets that formed in our example JSRES and EEJS simulations. The top panels show the growth of each surviving planet interior to 2 AU for the JSRES (left) and EEJS (simulations). The 50–150 Myr isotopic constraints on the timing of the Moon-forming impact on Earth are shaded. Each colored curve corresponds to an individual planet, as labeled. The bottom panels show the origin of the material incorporated into the planets. See Table 1 and the text for details.

The JSRES and EEJS simulations each reproduced some of our constraints but neither reproduced them all. The JSRES simulation formed a terrestrial planet system with eccentricities and inclinations almost as low as the Solar System's terrestrial planets', with an *AMD* of 0.0023 (as compared with 0.0018 for Mercury, Venus, Earth and Mars – hereafter MVEM). The JSRES planets also contain abundant water that was delivered from the primordial asteroid belt. The formation timescale of the Earth analog is roughly consistent with isotopic constraints for Earth. However, the JSRES Mars analog bears little resemblance to the real planet in terms of its mass and formation timescale. In addition, three extra large bodies exist at the end of the simulation: a 0.36 $M_\oplus$ planet at 1.8 AU and two embryos in the asteroid belt totaling 0.11 $M_\oplus$. These remnant bodies, in particular the embryos in the asteroid belt, are inconsistent with the observed inner Solar System.

The EEJS planets are novel among accretion simulations of this kind because they contain a reasonable Mars analog in terms of its mass, orbit and formation timescale. In addition, the approximate masses and spacing of the EEJS planets are close to those of Venus, Earth and Mars. No embryos are stranded in the asteroid belt although a dozen planetesimals remain in the belt. However, the EEJS Earth analog's formation timescale is too short by ~20%. More importantly, the *AMD* for the system is 0.0086, roughly 5 times higher than the MVEM value. Finally, the Earth analog is almost completely devoid of asteroidal water and thus requires an alternate source.

The values of the radial mass concentration statistic *RMC* of both simulations are far lower than for the inner Solar System. The *RMC* values are 28.5 for the JSRES simulation and 44.2 for the EEJS case, as compared with 89.9 for MVEM.

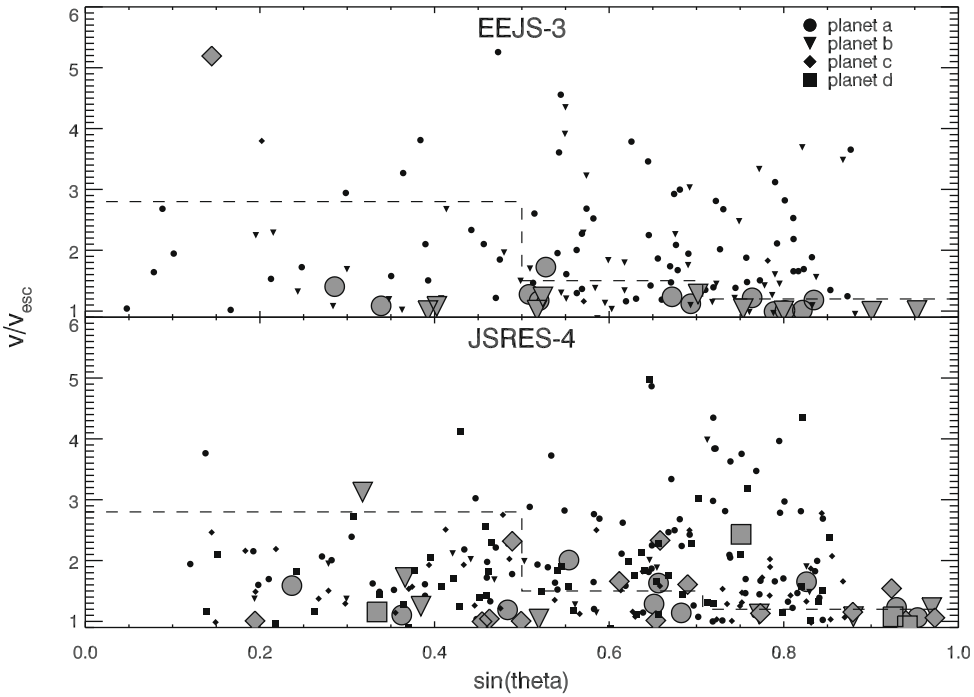

Fig. 6. Impact angles and velocities for all collisions that occurred in our example EEJS and JSRES simulations. Large grey symbols refer to embryo–embryo impacts and small black symbols to embryo–planetesimal impacts. Each symbol refers to the impacts that occurred on a specific planet – for each simulation, planets are ordered by their proximity to the star: planet a is closest, followed by planet b, etc. (the EEJS simulation only formed three planets so there is no planet d). Note that theta = 0 and 90° corresponds to head-on and graxing impacts, respectively. Impact velocities are normalized by the two-body escape speed v_{esc} (see Eq. (5)). The dashed line is the approximate boundary between accretionary (below the line) and erosive collisions (Agnor and Asphaug, 2004).

Fig. 6 shows the details of each planetesimal and embryo collision that occurred on the surviving planets in the two simulations. The impact angle theta is defined to be zero for a head-on collision and 90° for a grazing collision. The impact velocity is given in terms of the two-body escape speed v_{esc}:

$$v_{esc} = \sqrt{\frac{2G(M_1 + M_2)}{R_1 + R_2}}, \tag{5}$$

where G is the gravitational constant, M_1 and M_2 are the colliding bodies' masses, and R_1 and R_2 are the bodies' physical radii. In the absence of 3-body effects, which are relevant in at most a few percent of collisions, collisions can only occur at $v/v_{esc} > 1$.

Planetesimal-embryo impacts (small symbols in Fig. 6) tend to occur at higher velocities than embryo–embryo impacts simply because their eccentricities are higher on average due to viscous stirring. However, we expect virtually all planetesimal–embryo collisions to result in net growth. Note that our numerical scheme does not allow for planetesimal–planetesimal collisions (see discussion in Section 6).

High-speed or off-center embryo–embryo collisions (large symbols in Fig. 6) can result in either partial accretion or even erosion. Agnor and Asphaug (2004) showed that accretionary collisions only occur at $v/v_{esc} \lesssim 1.5$ and preferentially for small impact angles. The majority of giant impacts (filled circles in Fig. 6) occur at low speeds and should therefore be accretionary. Indeed, the majority of impacts lie in the accretionary regime as defined by Agnor and Asphaug (2004): 60%, 71%, 71%, and 75% for the four planets from the JSRES simulation (listed from closest- to farthest from the Sun), and 83%, 100% and 0% for the three EEJS planets.[6] This is a larger fraction than the 55% found by Agnor et al. (1999) and the ∼ half inferred by Agnor and Asphaug (2004). We assume that dynamical friction from small bodies reduced the mean impact speed and increased the fraction of accretionary impacts. We note, however, that the definition of an accretionary impact only requires that the collision produce an object larger than either of the two impactors, not that the object's mass equal the sum of the colliding masses. In particular, each of our example simulations has a cluster of impacts at low velocity but large angle (see discussion in Section 5). A large number of fragments is probably produced in these off-center collisions (Asphaug et al., 2006). We do not have the ability to track the effect of these fragments, which could be important (see discussion in Section 6). On the other hand, an erosive, "hit and run" collision usually results in an extra body that looks very similar to the original impactor and can easily be accreted in a later collision involving that extra body (Asphaug et al., 2006).

The different outcomes in the EEJS and JSRES example simulations can be attributed to differences in eccentricity and inclination excitation by specific resonances with Jupiter and Saturn, as well as by secular perturbations from Jupiter and Saturn. Fig. 7 shows the eccentricities of test particles on initially circular orbits after 1 Myr of evolution in each giant planet system, with no embryos present. For the JSRES case, the amount of eccentricity excitation is small. The main sources of excitation are the ν_5 secular resonance at 1.3 AU and the 2:1 MMR with Jupiter at 3.4 AU. The 3:1 and 3:2 MMRs with Jupiter are faintly visible at 2.6 and 4.1 AU. The small amount of external forcing means that the self-scattering of embryos and planetesimals is the dominant source of eccentricity in the JSRES simulations. Given that the disk is continuous and contains a significant amount of mass in the Mars region, no dynamical mechanism exists to remove that mass. In addition, the weak influence of the giant planets allows for efficient delivery of water-rich material via a large number of relatively weak embryo–embryo and embryo–planetesimal scattering events (Raymond et al., 2007).

[6] Note that for the outermost EEJS planet (the Mars analog), only one giant collision occurred, when the planet was just 0.036 $M_\oplus$ and was hit by a 0.015 $M_\oplus$ embryo. The collision was nearly head-on (sintheta = 0.14) but high-speed ($v/v_{esc} = 5.2$).

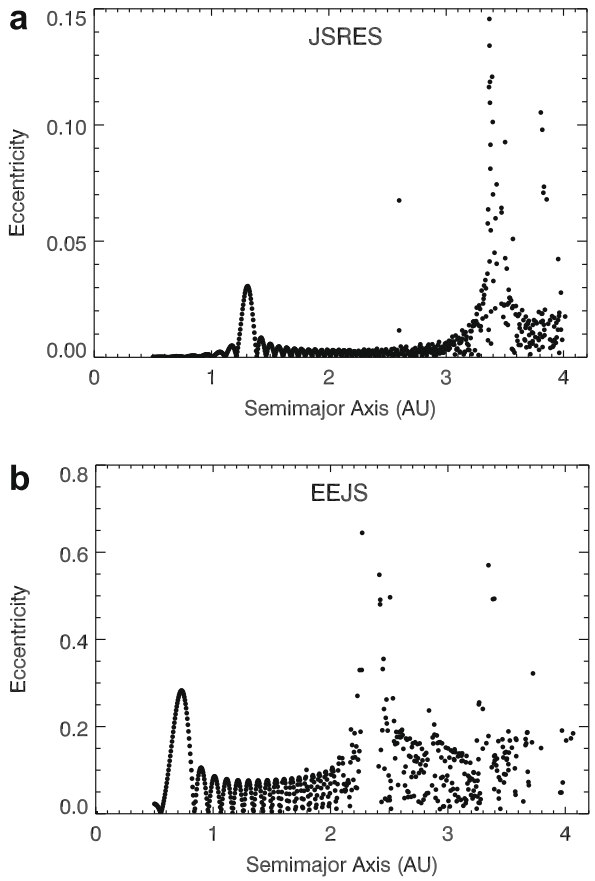

Fig. 7. Orbital eccentricities of massless test particles in the inner Solar System after 1 Myr for the JSRES (top panel) and EEJS (bottom panel) configurations of Jupiter and Saturn. Note the difference in the *y* axis scale between the two panels.

In contrast, perturbations from Jupiter and Saturn play a dominant role in the EEJS configuration (see Fig. 7). Strong secular resonances are visible at 0.7 AU (ν_5) and 2.2 AU (ν_6). In addition, secular excitation is strong enough to impart a typical free eccentricity of 0.1–0.2 throughout the inner Solar System. The ν_6 secular resonance is directly responsible for Mars' small size, as it efficiently removes mass from the 1.5–2.5 AU region, mainly by driving eccentricities of bodies to 1 and inducing collisions with the Sun. However, the ν_6 acts as a barrier between the terrestrial planets and the asteroid belt, such that water delivery is severely reduced. The strong eccentricity forcing throughout the inner Solar System appears to prevent low-*AMD* terrestrial planets from forming. However, the scattering of embryos and planetesimals by Jupiter and Saturn throughout accretion reduces the giant planets' eccentricities and weakens their secular perturbations in time.

Despite the differences between the JSRES and EEJS simulations, it is important to realize that small secular perturbations from the giant planets do not necessarily correlate with low-AMD terrestrial planets, especially in the case of limited numerical resolution. In fact, O'Brien et al. (2006) formed significantly lower-*AMD* terrestrial planets for the EJS configuration than their CJS simulations. The reason for this is that the timescale for the removal of asteroidal material was very long for the CJS simulations, and close encounters with late-arriving material from the asteroid belt tended to increase eccentricities. In contrast, their EJS simulations cleared out the asteroid belt quickly and the secular forcing of eccentricities was small enough inside ~2 AU that the giant planets did not act to increase the terrestrial planets' *AMD*.

5. Simulation outcomes and comparison with our constraints

The evolution of each simulation proceeded in a qualitatively similar fashion to the example EEJS or JSRES simulations. In fact, the two cases illustrated in Section 4 comprise the most extreme variations in our sample. The other cases lie between those extremes, typically with a moderate amount of excitation from the giant planets in the outer disk and relatively little external excitation in the inner disk. In this section we discuss the outcomes of our simulations in terms of how they compare with our Solar System constraints. We explore how the differences between cases can be attributed to the giant planet configuration and, to a lesser degree, to variations in the disk's density profile.

There was a large range in the characteristics of the terrestrial planet systems that formed. The number of planets in a given system ranged from 2–6, where we define a planet to contain an least one embryo, to be interior to 2 AU, and to be on a stable orbit that does not cross the orbit of any other planets or embryos. The total mass in planets varied by almost a factor of two, from 1.4 to 2.7 $M_\oplus$. Table 2 summarizes the outcome of each simulation.

Fig. 8 shows the median collision velocities and angles for the giant (embryo–embryo) collisions that occurred during the formation of the Earth and Mars analogs in each of our simulations.[7] Despite the existence of high-velocity impacts (see Fig. 6), the median collisional values are quite modest and in almost all cases the vast majority of giant collisions are accretionary rather than erosive.

If typical impact speeds or angles on Mars analogs were much higher than for Earth analogs, then the fraction of erosive collisions on Mars analogs would be higher and one could claim that the mass ratio of Mars- to Earth-analogs in our simulations was too high. However, the distribution of collision velocities for Earth and Mars analogs is very similar (Fig. 8). Therefore, we can rule out variations in impact properties as the source of large Mars analogs in our simulations. One exception are the EJS simulations, many of which have somewhat higher impact speeds and angles for Mars analogs than for Earth analogs. For the EJS simulations, the mass of Mars analogs may therefore be somewhat overestimated.

Canup (2004) showed that a very particular impact configuration was required to form the Moon. Such an impact must be low-velocity ($v/v_{esc} < 1.1$), off-center (sin[theta] between 0.67 and 0.76), and have an impactor to target mass ratio between 0.11 and 0.15. Canup (2008) found that, for prograde rotation of the proto-Earth, slightly smaller impactors can form Moon-analogs, with a cutoff at roughly 0.1. For retrograde rotation of the proto-Earth, larger impactor-to-target mass ratios are allowed but ratios less than 0.1 are still unable to form the Moon. We examined the last three giant impacts suffered by the Earth analog in each simulation, and none of the impacts fulfilled Canup's (2004) three requirements. In fact, none of the last three impacts on an Earth analog had an impactor to target mass ratio larger than 0.05 for the right collision angle and speed. In addition, only 4% of the late giant impacts satisfied Canup's velocity and angle criteria. We conclude that the Earth's Moon must be a cosmic rarity unless differences between planetary systems produce a systematic change in the likelihood of Moon-forming impacts. However, we note that the simulations of Canup (2004, 2008) were specifically designed to reproduce the details of the Earth–Moon system, in particular its high specific angular momentum and the Moon's small core. We suspect that a much larger range of late giant collisions would produce satellites, although their properties could be much different than the Moon.

[7] Earth and Mars analogs are defined to be the most massive planets in the region from 0.8 to 1.25 AU, and 1.25 to 1.75 AU, respectively. If no planet exists in that zone, then the Earth analog is taken to be the planet that is closest to 1 AU and the Mars analog is taken to be the outermost planet inside 2 AU.

Table 2
Comparison between simulations and observed constraints[a].

Simulation	N_p	M_{tot} ($M_\oplus$)	*AMD*	*RMC*	$WMF_\oplus$ (Earth)	M_{Mars}[b] ($M_\oplus$)	$Tf_\oplus$ (Myr)	Tf_M (Myr)	*N* (ast. emb.)
CJS15-1	3	2.70	0.0027	35.5	1.8×10^{-3}	1.45	50.7	113.7	2
CJS15-2	3	2.83	0.0107	27.3	5.7×10^{-3}	0.97	141.9	81.5	1
CJS15-3	4	2.89	0.0030	27.2	6.1×10^{-3}	0.98	75.0	113.6	0
CJS15-4	4	2.68	0.0030	29.8	5.3×10^{-3}	0.75	104.1	36.1	3
CJS1-1	2	2.30	0.0166	21.6	1.5×10^{-3}	1.05	149.7	186.3	2
CJS1-2	3	2.00	0.0315	44.8	7.9×10^{-3}	0.67	139.6	162.2	2
CJS1-3	4	2.45	0.0019	30.2	3.2×10^{-3}	0.89	33.3	100.3	0
CJS1-4	2	2.53	0.0104	27.8	2.1×10^{-3}	1.32	123.5	101.1	1
CJSECC15-1	3	2.20	0.0047	45.4	3.1×10^{-3}	0.58	80.4	63.8	1
CJSECC15-2	4	2.37	0.0053	34.9	1.2×10^{-3}	0.59	75.5	46.1	3
CJSECC15-3	4	2.42	0.0030	37.5	6.9×10^{-4}	1.09	96.3	164.1	5
CJSECC15-4	3	2.27	0.0010	40.9	9.3×10^{-4}	0.69	29.2	78.1	2
EJS15-1	3	2.08	0.0018	34.9	1.7×10^{-4}	0.81	56.1	76.3	2
EJS15-2	2	2.03	0.0025	48.9	3.3×10^{-4}	–	812.3	–	1
EJS15-3	3	2.05	0.0050	44.2	1.9×10^{-4}	0.26	38.9	118.3	1
EJS15-4	4	2.07	0.0062	34.7	2.6×10^{-4}	0.11	65.7	41.9	1
EJS1-1	2	1.66	0.0063	39.5	1.5×10^{-4}	0.75	147.8	303.7	1
EJS1-2	3	1.43	0.0101	46.0	6.3×10^{-3}	0.43	565.6	190.6	1
EJS1-3	3	1.60	0.0124	40.5	7.7×10^{-4}	0.22	142.0	548.6	1
EJS1-4	2	1.51	0.0035	51.2	1.4×10^{-2}	–	169.2	–	1
EEJS-1	3	1.83	0.0178	33.6	1.0×10^{-5}	0.34	109.3	59.6	1
EEJS-2	3	1.67	0.0151	50.9	1.1×10^{-4}	0.16	59.5	8.1	1
EEJS-3	3	1.66	0.0086	63.9	8.1×10^{-5}	0.06	35.6	0.2	0
EEJS-4	3	1.89	0.0112	43.6	2.1×10^{-5}	0.07	165.0	0.2	0
EEJS-5	4	1.78	0.0279	39.5	1.5×10^{-5}	0.34	102.3	128.1	0
EEJS-6	5	1.87	0.0099	39.4	2.9×10^{-5}	0.40	116.7	26.4	1
EEJS-7	3	1.85	0.0038	33.9	3.6×10^{-3}	0.44	129.4	98.3	2
EEJS-8	3	1.91	0.0248	31.6	8.6×10^{-3}	0.32	199.8	9.1	0
EEJS-9	5	1.83	0.0027	42.1	2.3×10^{-3}	0.23	33.1	91.3	1
EEJS-10	3	1.84	0.0047	42.6	1.9×10^{-5}	0.58	55.1	166.3	1
EEJS-11	4	1.72	0.0033	49.0	1.2×10^{-4}	0.09	145.0	4.5	1
EEJS-12	4	1.81	0.0027	44.9	2.5×10^{-4}	0.20	45.2	2.3	0
JSRES-1	6	2.61	0.0022	32.4	7.5×10^{-3}	0.54	29.2	28.1	2
JSRES-2	2	2.31	0.0119	61.0	5.3×10^{-3}	–	176.8	–	6
JSRES-3	4	2.55	0.0071	34.2	1.2×10^{-3}	0.57	115.3	18.1	1
JSRES-4	4	2.70	0.0023	28.5	2.9×10^{-2}	0.36	160.1	43.0	2
JSRESECC-1	4	2.70	0.0016	28.7	1.3×10^{-3}	1.01	20.2	81.0	1
JSRESECC-2	4	2.73	0.0044	26.8	3.5×10^{-4}	0.96	73.7	60.1	1
JSRESECC-3	4	2.51	0.0041	28.1	3.0×10^{-4}	0.73	78.5	99.8	3
JSRESECC-4	3	2.48	0.0025	39.3	1.1×10^{-3}	0.98	110.3	177.9	2
MVEM[c]	4	1.98	0.0018	89.9	$\sim 1 \times 10^{-3}$	0.11	50–150	1–10	0

[a] Table columns are: the simulation, the number of terrestrial planets inside 2 AU N_{pl}, the total mass in those planets M_{tot}, the angular momentum deficit *AMD* (see Eq. (2)), the radial mass concentration statistic *RMC* (see Eq. (1)), the water content by mass of the simulation's Earth analog $WMF_\oplus$, the mass of the simulation's Mars analog, the time of the last giant impact on the Earth and Mars analogs $Tf_\oplus$ and Tf_M, and the number of embryos stranded in the asteroid belt that were more massive than 0.03 $M_\oplus$. A comparison with the Solar System's terrestrial planets (MVEM) is shown at the bottom.

[b] Earth analogs were chosen as the largest planet between 0.75 and 1.25 AU. In a few rare cases when no planet formed in that interval, the Earth analog was chosen as the closest planet to 1 AU. Mars analogs were chosen to lie between 1.25 and 1.75 AU, although in a few cases they extended beyond 1.75 AU. A few simulations did not form Mars analogs at all (i.e., no planets between 1.25 and $\sim$ 2 AU).

[c] Earth's water content is not well known because the amount of water in the mantle has been estimated to be between 1 and 10 "oceans", where 1 ocean ($= 1.5 \times 10^{24} g$) is the amount of water on Earth's surface (+++Lécuyer et al., 1998). Our estimate of 10^{-3} for Earth's water content by mass assumes that 3 oceans are locked in the mantle.

As noted in Section 4, our simulations show a grouping of low-velocity grazing collisions. The difference between the velocity distributions at small and large angles is only significant for grazing collisions with sin(theta) > 0.9, where the collisions that were registered by the code do indeed occur at lower speeds. When comparing the statistics of head-on (sin[theta] < 0.7) and grazing (sin[theta] > 0.9) collisions in all 40 simulations, there were no notable differences in terms of collision time, distance from the Sun, or the details of the impactor. Grazing collisions did, however, have target masses $\sim$15% larger than for head-on collisions. Statistically, one would expect collisions between equal-mass objects to have a wider distribution in sin(theta) than for collisions with one dominant mass, although this also depends on the collision speed. The small mass ratio for the grazing collisions may explain the low collision speeds, simply because the two-body escape speed is larger than for unequal-mass objects.

It is possible that the `Mercury` code (Chambers, 1999) has difficulty registering high-speed grazing collisions because they could travel many Hill radii in a single timestep. For example, two bodies traveling with relative velocity of 10 km s^{-1} travel 0.035 AU with respect to each other in a single 6 day timestep. The Earth's Hill sphere R_H is about 0.01 AU, and approaches within $3R_H$ are tracked numerically with the Bulirsch-Stoer method rather than the symplectic map. Thus, any two objects that are flagged as having a close encounter will have their orbits faithfully resolved. However, if the two objects were never flagged to approach within $3R_H$ then an encounter could be missed. If that were the case then we would expect to miss more collisions at small orbital distances because the Hill sphere is smaller and relative velocities are larger. Although our statistics are limited, we do not see any evidence for this. On the other hand, the easiest grazing collisions for `Mercury` to find should be those between massive bodies traveling at low speeds, and we can think of no obvious physical reason that high-speed grazing collisions should not occur. Thus, although we have not found any evidence of the code missing high-speed grazing collisions, we can not rule out the possibility. We expect that such collisions would likely result in a "bounce" rather than a collision (Asphaug et al., 2006), and that later lower-speed or

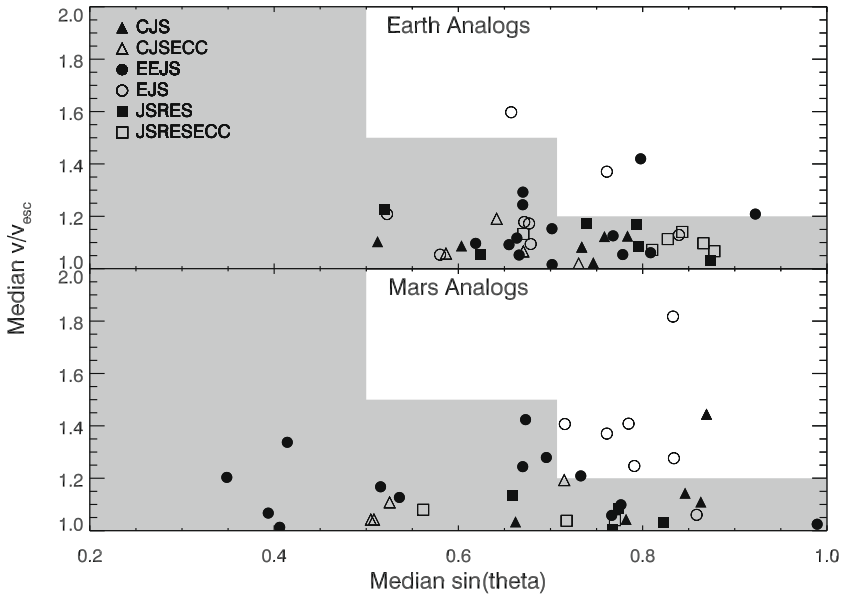

Fig. 8. Median angles and velocities for the giant collisions that formed the Earth and Mars analogs in each simulation, labeled with different symbols (see legend). The shaded region represents the zone where impacts should be accretionary rather than erosive (Agnor and Asphaug, 2004). Recall that theta = 0 and 90° corresponds to head-on and graxing impacts, respectively. Impact velocities are normalized by the two-body escape speed v_{esc} (see Eq. (5)).

Table 3
Mean properties of terrestrial planet systems for different disk surface density profiles[a].

Configuration	Mean N_p	Mean M_{tot} ($M_\oplus$)	Median *AMD*	Median $WMF_\oplus$	Median $T_{form,\oplus}$ (Myr)
CJS1	2.75	2.32	0.017	3.2×10^{-3}	140
CJS15	3.5	2.77	0.003	5.7×10^{-3}	104
EJS1	2.5	1.55	0.010	6.3×10^{-3}	169
EJS15	3.0	2.06	0.005	2.6×10^{-4}	66

[a] Recall that the CJS1 and EJS1 sims had disks with r^{-1} surface density profiles, while CJS15, EJS15, and all our other simulations had $r^{-1.5}$ surface density profiles.

head-on collisions, impacts that are certainly found by Mercury, would be the ones to result in planetary growth.

The effect of varying the disk's surface density profile between r^{-1} (i.e., $x = 1$) from Eq. (3) and $r^{-1.5}$ ($x = 3/2$) is not insignificant, although we only varied this parameter for the CJS and EJS configurations of Jupiter and Saturn (EJS1 and CJS1 had r^{-1}, EJS15 and CJS15 had $r^{-1.5}$). The properties of the CJS1, CJS15, EJS1 and EJS15 simulations are summarized in Table 3. The r^{-1} simulations formed slightly fewer planets, contained less total mass in planets, had longer formation timescales for Earth and higher *AMD* values for the final systems than the $r^{-3/2}$ simulations. In addition, Earth analogs in the EJS1 simulations contained far more water than Earths in the EJS15 simulations.[8] These trends are consistent with the results of Raymond et al. (2005), and appear to be due simply to the fact that the r^{-1} simulations contain far more mass in the asteroid region than the $r^{-1.5}$ simulations. Given that planets form largely from local material, the r^{-1} simulations contain less material in the inner disk and therefore form less massive planets. In addition, the relatively large amount of water-rich material in the asteroid belt increases the probability of water delivery, although water delivery is more sensitive to the giant planet configuration than to the disk properties: despite the large median value, note that 2/4 EJS1 simulations formed Earths with less than 1 part per thousand of water (see Table 2). The large amount of asteroidal material in the r^{-1} simulations also prolongs the period of chaotic bombardment, increasing the mean formation time for Earth.

The higher *AMD* values for r^{-1} simulations appears to be linked to the mean formation timescale. Indeed, Fig. 9 shows a weak correlation between the timescale for the last giant impact on Earth $T_{form,\oplus}$ and the *AMD* of the system for all 40 simulations. For $T_{form,\oplus} < 100$ Myr, the median *AMD* is 0.003 and for $T_{form,\oplus} > 100$ Myr, the median *AMD* is 0.010. We attribute this trend to the fact that the planetesimal population decays with time and our simulations have limited resolution. So for late giant impacts or scattering events among the embryos, there are fewer planetesimals around to re-damp the planets by dynamical friction if the planets form more slowly. This problem could be alleviated with simulations which continuously regenerate planetesimals from the debris of giant impacts (e.g., Levison et al., 2005), because in that case the planetesimal population would be sustained for as long as the giant impacts occur.

For the remainder of our analysis we consider the giant planet configuration as the only variable. We therefore combine the CJS1 and CJS15 simulations into CJS, and the EJS1 and EJS15 cases into EJS. Given that the failings of these simulations are generally the same (see Table 2), we do not expect this to skew our results.

Fig. 10 shows the mass-semimajor axis distribution of all 40 of our simulations, grouped into categories with similar giant planet configurations. When compared with the Solar System's terrestrial planets, it is immediately evident that all cases with circular or

[8] The same trend was not seen in the CJS1 vs. CJS15 simulations because the small number of planets that formed in the CJS1 cases led to the Earth analog being located at ~0.8 AU in 3/4 cases. Given that water delivery decreases with distance from the water source (> 2–2.5 AU), this decreased the water content of Earth analogs in the CJS1 simulations.

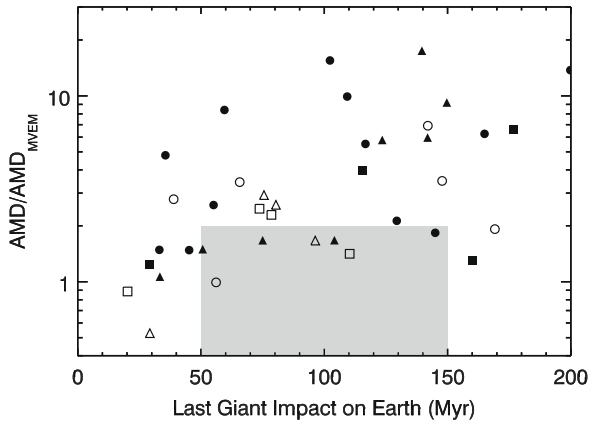

Fig. 9. The system angular momentum deficit, normalized to the MVEM value of 0.0018, as a function of the time of the last giant impact for the Earth analog in each of our simulations. The symbol for each simulation is the same as in Fig. 8. The region of successful outcomes is shaded.

lower-eccentricity giant planets fail miserably at reproducing Mars' small size. Indeed, for the CJS, CJSECC, JSRES and JSRESECC simulations, planets in Mars' vicinity are typically 0.5—1 $M_\oplus$. The radial distribution of massive planets is much broader in these cases than in the Solar System, and Earth-sized planets are commonly formed all the way out to 2 AU. In contrast, the EJS and especially the EEJS simulations did a much better job of reproducing Mars' small size. The EJS simulations have smaller Mars analogs than the CJS and JSRES cases but in most cases $M_{Mars} \approx 0.3\ M_\oplus$. In 5/12 EEJS simulations the Mars analog was between 0.06 and 0.2 $M_\oplus$, and in each of those five cases the last giant impact occurred before 10 Myr. The radial mass distributions for the EJS and EEJS simulations are peaked, as is the case for MVEM. For the EJS simulations the peak is close to (or perhaps slightly interior to) 1 AU, but for the EEJS simulations the most massive planets tend to lie interior to 1 AU and planets at 1 AU are typically half an Earth mass. This can be explained as a byproduct of the excitation of the planetesimals and embryos by the giant planets: planetesimals and embryos on eccentric orbits are most likely to collide close to perihelion, such that systems with eccentric giant planets tend to have the most massive planets closer to their stars than for systems with low-mass or low-eccentricity giant planets (Levison and Agnor, 2003).

It is also clear from Fig. 10 that simulations with circular or low-eccentricity giant planets (CJS, CJSECC, JSRES, JSRESECC) tend to strand massive embryos in the asteroid belt. These embryos are typically 0.05—0.2 $M_\oplus$ and would certainly disrupt the observed asteroid distribution. In contrast, the EJS and EEJS simulations leave fewer embryos in the asteroid belt, and those that are stranded are typically smaller.

A trend that is less evident from Fig. 10 is that the total terrestrial planet mass decreases with the giant planet eccentricity in almost all cases. The one exception to this rule is for the JSRESECC simulations, which have roughly the same total planet mass as the JSRES cases; however, at the end of each JSRESECC simulation $e_J < 0.01$, so the difference between the two giant planet configurations is actually fairly minor. The reason for the correlation between increased giant planet eccentricity and decreased total mass in terrestrial planets is simply that eccentric giant planets perturb terrestrial and asteroidal bodies more strongly and destroy a larger fraction of the disk via ejection and collisions with the Sun than circular giant planets (Chambers and Cassen, 2002; Levison and Agnor, 2003; Raymond et al., 2004; O'Brien et al., 2006). In addition, terrestrial planets cannot form as close to eccentric giant planets as they can to circular giant planets (Raymond, 2006); this

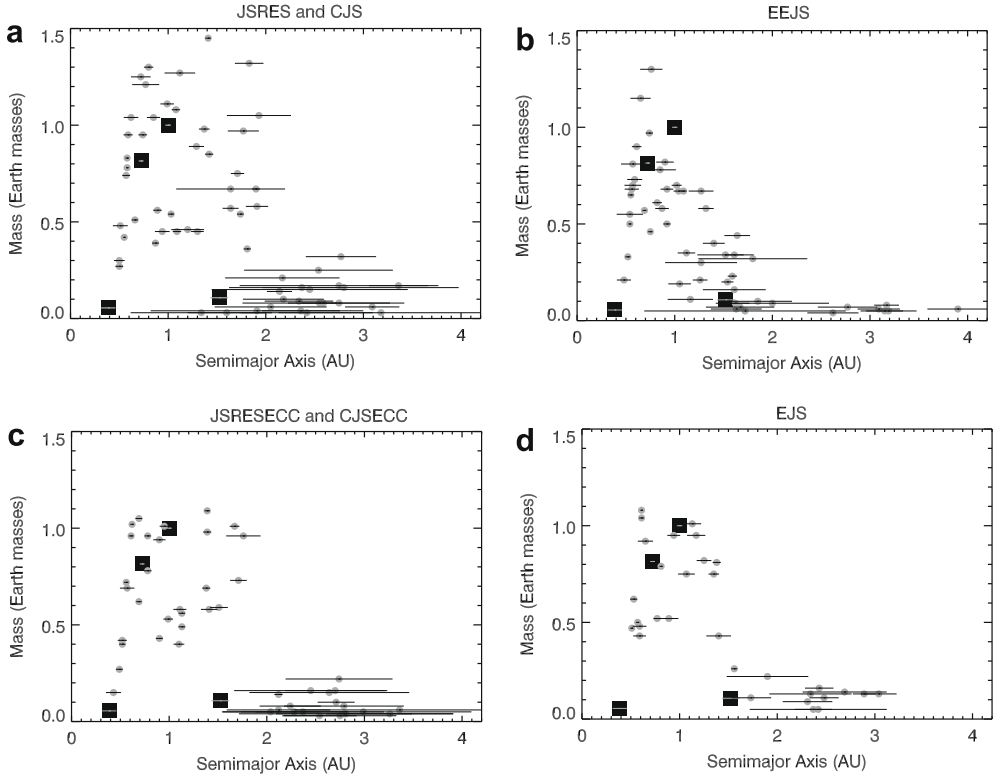

Fig. 10. Mass vs. semimajor axis for a range of simulations with different configurations of Jupiter and Saturn. Each panel shows all planets that formed in the relevant simulations (see Table 2) as grey circles, with horizontal lines representing the orbital eccentricity. The Solar System's terrestrial planets are shows as the black squares, with 3 Myr averages for their eccentricities in grey (taken from Quinn et al., 1991).

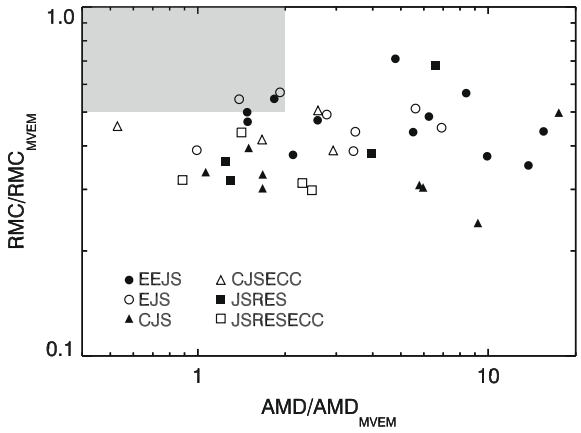

Fig. 11. The angular momentum deficit *AMD* (Eq. (2)) vs. radial mass concentration statistic *RMC* (Eq. (1)) for all of our simulations. Both the *AMD* and *RMC* are normalized to the MVEM values of 0.0018 (*AMD*) and 89.9 (*RMC*). The terrestrial planet system from each simulation is represented as a single point, following the label at the bottom of the plot (e.g., EEJS simulations are filled circles, etc.). The region of successful outcomes is shaded.

may explain the reduced number of stranded asteroidal embryos for the EJS and EEJS simulations.

Fig. 11 shows the radial mass concentration statistic *RMC* as a function of the angular momentum deficit *AMD* for the terrestrial planet system that formed in each simulation. These statistics are normalized with respect to the MVEM values of 0.0018 and 89.9. The systems that formed have a wide range in *AMD*, from 0.5 to almost 20 times the MVEM value. In contrast, systems are clumped in *RMC* between 0.3 and 0.7 times the MVEM value; none has *RMC* higher than 0.71 – this is similar to the results of Chambers (2001). Most systems have *AMD* values somewhat larger than MVEM, although a few cases have *AMD* smaller than MVEM (see Table 2).

Table 4 lists the median *AMD* and *RMC* values for each giant planet configuration. The *AMD* varies significantly for the different configurations, and is smallest for the JSRESECC and CJSECC simulations. This is consistent with the results of O'Brien et al. (2006), who formed lower-*AMD* systems for cases with moderately eccentric giant planets (analogous to our EJS simulations). The most eccentric planets formed in the CJS and EEJS simulations. The CJS systems were eccentric because the timescale for clearing out of the asteroid belt and late encounters with remnant embryos was relatively long such that few planetesimals remained for damping after late encounters, as discussed above. The EEJS systems were eccentric mainly because of the excitation caused by the ν_5 and ν_6 resonances, as well as direct perturbations by the giant planets. However, our numerical resolution also played a significant role: the four EEJS simulations with 1000 planetesimals (EEJS 1–4) had a median *AMD* of 0.015, but the four simulations with 2000 planetesimals and slightly less eccentric giant planets (EEJS 9–12) had a median *AMD* of 0.0033. Note, however, that the EEJS terrestrial planet systems with 2000 planetesimals and $e_J = e_S = 0.1$ (EEJS 5–8) were even slightly more eccentric than the cases with 1000 planetesimals. This large variation in *AMD* for the EEJS cases is again linked to the presence or absence of damping at the time of the last encounters between embryos. Indeed, the mean formation timescale for Earth analogs again scales inversely with the *AMD*: for EEJS 1–4, 5–8, and 9–12 the median formation timescales for Earth were 109, 129, and 55 Myr. This continues an important trend that we see: longer formation timescales lead to higher *AMD* because fewer planetesimals exist for dynamical friction at later times. This trend is caused in part by our numerical resolution (1000–2000 planetesimals instead of billions) and in part because we do not account for impact debris. However, the planetesimal population certainly does contribute to decreasing eccentricities so we believe that this effect is real, although accounting for other factors should weaken the correlation.

We performed a suite of two-sided Kolmogorov-Smirnov and Wilcoxon tests to determine which differences in *AMD* and *RMC* in our simulations were statistically significant. At the 0.05 level (i.e., $p < 0.05$ where p is the probability that the two distributions were drawn from the same sample), we only found differences between the EEJS normal-resolution simulations (EEJS 1–4 = EEJSnr [with 1000 planetesimals], EEJS 5–12 = EEJShr [2000 planetesimals]) and CJSECC, EJS15, and JSRESECC, all with $p < 0.029$ from Wilcoxon tests. For the *RMC* values, the following sets of simulations provided significantly different values ($p < 0.05$): CJS15 vs. EJS1 ($p < 0.029$), CJS15 vs. EEJShr ($p < 0.016$), EEJShr vs. JSRESECC ($p < 0.016$), and EJS1 vs. JSRESECC ($p < 0.029$). If we only include variations of giant planet configuration and ignore changes in disk surface density profile (for the CJS and EJS simulations) and resolution (for the EEJS simulations), there are no statistically significant differences in *AMD*, but for *RMC* there are differences between the following configurations: CJS vs. CJSECC ($p < 0.048$), CJS vs. EJS ($p < 0.007$), CJS vs. EEJS ($p < 0.005$), EJS vs. JSRESECC ($p < 0.016$), and EEJS vs. JSRESECC ($p < 0.008$). Thus, the normal-resolution EEJS simulations have significantly higher *AMD* values than the other simulations, but increasing the resolution brings them into agreement with the other cases (just as increasing the resolution for the other cases would likely also decrease their *AMD* values). The CJS (especially CJS15) and JSRESECC simulations represent the statistically smallest *RMC* values of our sample, and the highest come from the *EJS* and *EEJS* simulations, although these are still far below the MVEM value.

We follow Thommes et al. (2008) and define a successful outcome as a system for which both the *AMD* and *RMC* are within a factor of two of the MVEM values. This successful area is shaded in Fig. 11. Only four simulations were successful in terms of *AMD* and *RMC*, and all had relatively eccentric giant planets: EJS1-4, EJS15-2, EEJS-11 and EEJS-12.

Table 4
Statistical values of terrestrial planet systems for different giant planet configurations.

Giant planet configuration	Mean N_p	Median *AMD*	Median *RMC*	Median $WMF_\oplus$	Median $T_{form,\oplus}$ (Myr)
CJS	3.13	0.010	29.8	5.3×10^{-3}	123.5
CJSECC	3.5	0.0047	40.9	1.2×10^{-3}	80.4
EJS	2.75	0.0062	44.2	3.3×10^{-4}	147.8
EEJS[a]	3.58	0.0099	42.6	1.1×10^{-4}	109.3
JSRES	4	0.0071	34.2	7.5×10^{-3}	160.1
JSRESECC	3.75	0.0041	28.7	1.1×10^{-3}	78.6
Solar System	4	0.0018	89.9	$\sim 10^{-3}$	50–150

[a] Note that there were 12 EEJS simulations, including 8 with 2000 planetesimals. For the 4 EEJS simulations with 1000 planetesimals (EEJS 1-4), the median $N, AMD, RMC, WMF_\oplus$ and $T_{form,\oplus}$ were 3, 0.015, 50.9, 8.1×10^{-5}, and 109.3 Myr, respectively.

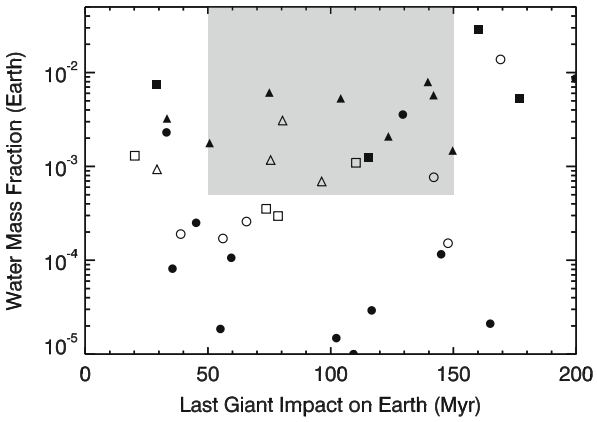

Fig. 12. The water content by mass $WMF_\oplus$ vs. the time of the last giant impact for the Earth analog in each of our simulations. The symbol for each simulation is the same as in Fig. 11. Also as in Fig. 11, the region of successful outcomes is shaded.

Fig. 12 shows the water content by mass $WMF_\oplus$ of the Earth analog in each simulation vs. the time of the last giant impact on that same planet $T_{form,\oplus}$. There is a wide range in both of these parameters, and some correlation with the giant planet configuration (see Table 3). As expected, the majority of dry planets come from the EJS and EEJS samples.

We define a successful outcome in Fig. 12 to have $T_{form,\oplus} = 50$–150 Myr $WMF_\oplus > 5 \times 10^{-4}$. The water constraint requires two oceans of water to have been accreted by the planet, because Earth's minimum bulk water content is two oceans, one on the surface and one in the mantle (Lécuyer et al., 1998; 1 ocean $= 1.5 \times 10^{24}$ g is the amount of water on Earth's surface). Of our 40 simulations, 14 were successful in $WMF_\oplus - T_{form,\oplus}$ space, but there was no overlap with the 4 successful cases from $RMC - AMD$ space. The CJS and CJSECC cases were the most successful in this respect: 10/12 CJS and CJSECC simulations satisfied both the $WMF_\oplus$ and $T_{form,\oplus}$ constraints.

6. Discussion and conclusions

In this section we first discuss the degree to which each giant planet configuration was able to reproduce our observed constraints (Section 6.1). Next, we discuss the context of each giant planet configuration in terms of the Solar System as a whole (Section 6.2). We then point out the limitations of our simulations, and plans for future work (Section 6.3).

6.1. Success of giant planet configurations in satisfying our constraints

Let us quantitatively evaluate how the simulations fared at reproducing our five constraints using relatively generous values: (1) $M_{Mars} < 0.3\ M_\oplus$, (2) $AMD < 0.0036$ (twice the MVEM value), (3) 50 Myr $< T_{form,\oplus} <$ 150 Myr, (4) less than 0.05 $M_\oplus$ in embryos is stranded in the asteroid belt, and (5) $WMF_\oplus > 5 \times 10^{-4}$. No single simulation reproduced all five constraints. Three simulations reproduced four constraints. The simulation CJS15-3 reproduced four constraints, but formed a 0.98 $M_\oplus$ Mars analog at 1.37 AU and a 0.58 $M_\oplus$ planet at 1.91 AU. The simulation EJS1-3 formed a small Mars, a wet Earth on the correct timescale, and stranded one, 0.048 $M_\oplus$ embryo in the asteroid belt, but the system's AMD is far too large (0.012). The simulation EEJS-9 formed a small Mars, low-AMD planets and a wet Earth with one 0.04 $M_\oplus$ embryo in the main belt. Many simulations reproduced three constraints, but rarely while forming a small Mars. As expected from previous work, Mars' small size was the most difficult constraint to reproduce, and no simulations outside of the EJS and EEJS configurations form a single Mars analog less massive than 0.5 $M_\oplus$.

Table 5
Summary of the success of Jupiter–Saturn configurations for reproducing inner Solar System Constraints[a].

Config.	AMD	M_{Mars}	T_{form}	Ast. Belt	$WMF_\oplus$
CJS	✓	×	✓	~	✓
CJSECC	✓	×	✓	×	✓
EJS	✓	~	✓	~	~
EEJS	✓	✓	~	✓	~
JSRES	✓	×	~	×	✓
JSRESECC	✓	×	✓	×	✓

[a] For each configuration of Jupiter and Saturn, a check ("✓") represents success in reproducing a given constraint in at least half the simulations, a cross ("×") represents a failure to reproduce the constraint in any simulations, and a twiddle sign ("~") represents a "maybe", meaning success in reproducing the constraints in a smaller fraction of cases.

Table 5 crudely summarizes the outcomes of our simulations in terms of the likelihood of a system with a given giant planet configuration's ability to quantitatively reproduce our observed constraints using the values above. We completed the table as follows. A configuration is said to reproduce a given constraint (and receives a "✓") if at least half of the simulations were successful for that constraint, using the constraints listed immediately above. A configuration is unsuccessful at reproducing a constraint (and receives a "×") if no simulations are successful. If isolated cases or a small fraction of simulations are successful, then the configuration receives a maybe ("~"). In one case we bent these rules; 5/12 EEJS simulations formed a Mars analog smaller than 0.3 $M_\oplus$ (four cases $< 0.2\ M_\oplus$) so we gave EEJS a ✓ for this constraint despite a slightly less than 50% success rate.

The most successful giant planet configuration was EEJS ("Extra-Eccentric Jupiter and Saturn"). The EEJS simulations reliably satisfied three of our constraints with two maybes (see Table 5), and the ensemble of EEJS simulations satisfied all five constraints, although no single simulation did so. The EEJS cases reliably formed reasonable Mars analogs in terms of Mars' mass, orbit, and formation timescale. Planetary eccentricities were too large in most cases, but increasing the number of planetesimals (runs EEJS 5-12) decreased the AMD to close to the MVEM value, and even higher resolution simulations would presumably continue decrease the AMD to the MVEM value. The Earth analog formed on the correct, 50–150 Myr timescale in most EEJS simulations but was too dry in all but three cases. Almost half (5/12) of the EEJS simulations finished with no embryos in the asteroid belt, and for the cases with trapped asteroidal embryos they were typically low mass. However, we note that for the EJS and EEJS configurations the survival of any embryos in the asteroid belt constitutes a failure because Jupiter and Saturn's orbits do not allow for any migration, which would be necessary to clear remaining embryos from the belt – this issue is discussed further in Section 6.2.

The main reason for the success of the EEJS simulations was the strength of the ν_6 secular resonance located at ~2 AU, which created an "edge" to the inner disk, effectively separating it from the asteroid region, removing material that approached 2 AU and thereby helping to form a small Mars. The high eccentricities of Jupiter and Saturn ($e_{Jup,Sat} = 0.07$–0.10) were responsible for the strength of the resonance; the EJS simulations had ν_6 in the same place but it was too weak to clear out enough material to form a small Mars. However, having the ν_6 at this location also makes it difficult for water-bearing asteroidal material to enter the inner Solar System and be accreted by the terrestrial planets.

In several of the giant planet configurations that we considered – CJS, CJSECC, JSRES, and JSRESECC – Jupiter and Saturn had lower eccentricities than their current values. For all of these simulations,

the Earth generally formed on the correct timescale and the terrestrial planets were low-eccentricity and water-rich. However, not a single simulation from these four cases was able to reproduce Mars' small size, and most simulations stranded one or more large embryos in the asteroid belt. Therefore, this work suggests that low-eccentricity configurations of Jupiter and Saturn cannot explain the terrestrial planets, in particular Mars' small size, in the context of our simulations.

It is interesting that none of our simulations was able to reproduce the large radial mass concentration seen in the Solar System's terrestrial planets (*RMC* = 89.9 for MVEM vs. 30–50 for most simulations; see Fig. 11 and Eq. (1)). This concentration comes from the large masses and proximity of Venus and Earth, and the small masses of Mercury and Mars. Given the difficulty in producing Mars analogs, it is not surprising that simulations with low-eccentricity giant planets yield small *RMC* values. However, the EEJS and EJS simulations also yielded *RMC* values far smaller than MVEM, although larger than for the other giant planet configurations. The origin of this discrepancy is not clear. It could be related to the structure of the planetesimal disk; observations suggest that inner, dust-free cavities exist in many disks around young stars with varying radii, from < 0.1 to ~ 1 AU. (e.g., Eisner et al., 2005; Millan-Gabet et al., 2007). If the Solar Nebula had a large inner cavity then the inner boundary for the planetesimal disk could have been at roughly Venus' orbital distance such that the radial compression of MVEM is a result of accretion in a radially compressed planetesimal disk. Alternately, resonant sweeping or tidally-induced migration from interactions with the residual gas disk or perhaps collisional debris could compress the terrestrial planet system and increase the *RMC* (see Thommes et al., 2008). However, a difficulty with this model is that Earth's formation timescale is much longer than the typical gas disk lifetime (see Section 6.3).

6.2. Putting the giant planet configurations in the context of the solar system

Our giant planet configurations, described in Section 3.1, represent different assumptions about the early evolution of the Solar System. Four of our cases – CJS, CJSECC, JSRES, and JSRESECC – are based on the Nice model, which requires Jupiter and Saturn to have formed interior to their mutual 2:1 mean motion resonance (Tsiganis et al., 2005; Morbidelli et al., 2007). These four cases assume that delayed, planetesimal scattering-driven migration spread out the giant planet system, and that the 2:1 resonance crossing of Jupiter and Saturn triggered the late heavy bombardment (Gomes et al., 2005; see also Strom et al., 2005). The other two giant planet configurations – EJS and EEJS – have Jupiter and Saturn at their current semimajor axes, meaning that planetesimal-scattering driven migration is not permitted because this inevitably leads to spreading out of the giant planets' orbits (Fernandez and Ip, 1984). Therefore, the EJS and EEJS simulations assume that the Nice model is incorrect and that the late heavy bombardment was caused by another mechanism. The only other currently-viable such mechanism is the "planet V" theory of Chambers (2007) which invokes the formation and delayed instability of a fifth, sub-Mars mass terrestrial planet at ~ 2 AU. Thus, for EEJS and EJS simulations to be consistent with the Solar System's observed history they must form a planet V with the right mass ($\lesssim M_{Mars}$) and in the right location (~ 2 AU).

Our results clearly favor the EEJS simulations over giant planet configurations that are consistent with the Nice model, mainly because of the EEJS simulations' ability to form Mars analogs. In addition, the constraints that were poorly reproduced by the EEJS simulations were in some sense our weakest, because higher resolution simulations with more planetesimals tend to lower the *AMD*, and alternate models exist for water delivery to Earth (e.g., Ikoma and Genda 2006; Muralidharan et al., 2008). Moreover, EEJS simulations 5, 6 and 11 formed reasonable planet V analogs (see Table 2). In one of these cases, simulation EEJS-11, a good Mars analog formed at 1.62 AU and a 0.09 $M_\oplus$ planet V formed at 2.0 AU. Given the significant inclination of the planet V in this case (12°), the instability timescale could be several hundred Myr (e.g., Morbidelli et al., 2001). That simulation therefore may represent the most self-consistent simulation in our sample, at least when only considering the inner Solar System constraints.

Given that planets are thought to form on circular orbits (e.g., Pollack et al., 1996), what would be the source of the significant eccentricities of Jupiter and Saturn in the EEJS configuration? Goldreich and Sari (2003) proposed that eccentricities of Jupiter-mass planets could be excited by lindblad resonances in gaseous protoplanetary disks, but with eccentricities limited by the width of the gap carved out of the disk by the planet. D'Angelo et al. (2006) found that planets embedded in eccentric disks can have their eccentricities increased to $\sim$0.1. However, other studies have shown that eccentricity growth via planet-disk interactions can only occur for very massive, $> 10 M_{Jup}$ planets (Papaloizou et al., 2001; Kley and Dirksen, 2006). Thus, the origin of EEJS-type configurations of Jupiter and Saturn remains controversial but certainly within the realm of current thinking.

Another study has shown that the EEJS configuration may be advantageous for reproducing the inner Solar System. Thommes et al. (2008) also took advantage of strong secular resonances to reproduce the terrestrial planets. In their model, collisions between embryos were induced by the inward sweeping of the ν_5 and ν_6, which occurred as the Solar Nebula dissipates and changes the gravitational potential (Heppenheimer, 1980; Ward, 1981). Their source of damping is tidal interaction with the gas (Ward, 1993; Cresswell et al., 2007). They manage to reproduce several aspects of the terrestrial planets, including Mars' small size. However, we note that Thommes et al. (2008) assumed that the inner disk only contained embryos out to 3 AU and no planetesimals.

Given these successes, it is tempting to regard the EEJS configuration as the true configuration of Jupiter and Saturn early in Solar System history. EEJS is indeed consistent with the inner Solar System. In the EEJS scenario, Jupiter and Saturn must have acquired eccentricities of $\sim$0.1 at an early stage, within 1 Myr or so after their formation. Scattering of unstable planetesimals and embryos over the $\sim 10^8$ years of terrestrial accretion decreased their eccentricities to their current values of $\sim$0.05. Indeed, the final time-averaged values of e_{Jup} and e_{Sat} in our simulations are 0.03–0.06 and 0.06–0.10, respectively, very close to their current orbits. In this model, Earth's water was delivered in part from hydrated asteroidal material, but mainly from adsorption of small silicate grains (Muralidharan et al., 2008), cometary impacts (Owen and Bar-Nun, 1995) or oxidation of a H-rich primitive atmosphere (Ikoma and Genda 2006). The late heavy bombardment of the terrestrial planets can then be explained by the delayed destabilization of planet V (Chambers, 2007), analogs of which did indeed form in several EEJS simulations.

The outer Solar System provides a strong argument against the EEJS configuration. The resonant structure of the Kuiper Belt requires outward migration of Neptune (Malhotra, 1993, 1995; Levison and Morbidelli, 2003). It is thought that Neptune migrated outward because of the back-reaction from the scattering of a many Earth masses worth of remnant planetesimals. Given that Neptune cannot easily eject these planetesimals (e.g., Duncan et al., 1987), the scattering of these small bodies also causes Uranus and Saturn to migrate outward, and Jupiter, which does eject most of the small bodies, to migrate inward (Fernandez and Ip, 1984; Hahn and Malhotra, 1999). This planetesimal scattering is thought to have started during planet formation and lasted for 10^7–10^9 years, with more rapid migration corresponding to a more massive

planetesimal disk or closer proximity between Neptune and the disk's inner edge (Gomes et al., 2004; Gomes et al., 2005). Excess depletion just exterior to strong resonances in the asteroid belt provides empirical corroboration of giant planet migration (Minton and Malhotra, 2009), although the migration timescale cannot be constrained. Thus, the current orbits of Jupiter and Saturn are not thought to be their orbits at the time of formation, and it is their orbits at early times that affected terrestrial planet formation. In particular, Jupiter and Saturn must have formed in a more compact configuration, because scattering-induced migration always causes their orbits to diverge.

Is it possible to reconcile the EJS and EEJS configurations with the outward migration of Neptune that is required by current Kuiper Belt models? If a small Mars formed because of the ν_6 resonance, then the ν_6 must have been in roughly its current location during Mars' formation. Hf/W isotopes suggest that Mars formed much faster than Earth, and did not undergo any giant impacts after 1–10 Myr (Nimmo and Kleine, 2007). In addition, the location of the ν_6 is highly sensitive to Jupiter and Saturn's semimajor axes such that a more compact configuration places the ν_6 in the asteroid belt, farther from Mars and less likely to influence its growth (see Fig. 1 of Minton and Malhotra, 2009). Migration of Jupiter and Saturn must therefore have been completely finished in a few Myr at the latest to form a small Mars. Would such an early migration fit our current understanding? At such early times there likely existed a population of embryos in the asteroid belt (Wetherill, 1992). If Jupiter and Saturn's migration occurred that early, then embryos would probably have smeared out the observed depletion of asteroids exterior to asteroid belt resonances (Minton and Malhotra, 2009). In addition, this very rapid migration must also have taken place in the presence of some amount of residual disk gas, which would certainly have affected the scattering dynamics (Capobianco et al., 2008), and would likely have been far too efficient in trapping Kuiper Belt objects in resonances with Neptune (e.g., Mandell et al., 2007). This suggests that the EEJS configuration is at best marginally consistent with the outward migration of Neptune needed by models of the Kuiper Belt. Neptune's migration would have to have occurred early and been very rapid. In addition, to remain consistent with the late heavy bombardment, a fifth terrestrial planet must have formed at ~2 AU (Chambers, 2007).

An alternate hypothesis for the evolution of the outer Solar System suggests that there initially existed several additional ice giant planets (Chiang et al., 2007). Could such a scenario be consistent with the EEJS configuration? In this model, instabilities among the ice giants would have led to the ejection of excess ice giants and dynamical friction could re-circularize the orbits of Uranus and Neptune (Ford and Chiang, 2007). However, in order to avoid disrupting the EEJS configuration by injecting planetesimals into the Jupiter–Saturn region, those planetesimals would need to have been dynamically ejected by the ice giants themselves, which is unlikely given their relatively small masses. In addition, a detailed simulation of this model suggests that a population of many ice giants would not eject each other but would simply spread out by interactions with the planetesimal disk (Levison and Morbidelli, 2007). Thus, we are left with the same issue, that the giant planets would have had to clear out the outer Solar System in less than Mars' formation timescale of a few Myr. This scenario therefore does not appear to be consistent with the EEJS configuration.

The Oort cloud provides an additional argument against the EEJS configuration. If the giant planets reached their current orbits very quickly (as required by EEJS), then the Oort cloud had to form very quickly as well. To populate the inner and outer classical Oort cloud, the current galactic environment (or one moderately denser) is required (Brasser et al., 2006; Kaib and Quinn, 2008). However, to capture Sedna (Brown et al., 2004), a significantly denser environment is needed. These two constraints are not at odds if the giant planets evolved on long timescales, because the galactic environment can change on a 10–100 Myr timescale (e.g., Lamers et al., 2005). However, if the giant planets finished migrating, and therefore finished clearing the planetesimal disk, within a few Myr, then the Solar System should have either an Oort cloud *or* Sedna, but not both.

Thus, we are left with a problem: the giant planet configuration which best reproduces the terrestrial planets (EEJS) is at best marginally consistent with the current view of the outer Solar System's evolution, and likely inconsistent. On the other hand, configurations that are based on current outer planet evolution models, in particular the Nice model, cannot form a small Mars, an inescapable inner Solar System constraint. Given that we do not have a choice for the configuration of Jupiter and Saturn at early times that satisfies all of our constraints and is also consistent with the evolution of the outer Solar System, we cannot reject the Nice Model.

6.3. Simulation limitations and future work

It is important to note that our simulations are missing several physical effects that could be important. These effects include collisional fragmentation (Alexander and Agnor, 1998), dynamical effects of collisional debris (Levison et al., 2005), tidal damping and resonant sweeping from a residual amount of nebular gas (Kominami and Ida, 2002; Nagasawa et al., 2005; Thommes et al., 2008).

We do not think that including collisional fragmentation would affect our results for two reasons: (1) Alexander and Agnor (1998) saw little difference in their simulations when they included a simple fragmentation model, and (2) the velocities of embryo–embryo collisions were slow enough that the majority were accretionary rather than erosive (Agnor and Asphaug, 2004).

We also assumed that all embryo–planetesimal impacts were accretionary, although these do tend to occur at larger velocities than embryo–embryo impacts because of viscous stirring (see Fig. 6). Melosh (1984) showed that it is difficult for km-sized impactors to accelerate material to speeds greater than one third of the impact speed. Based on this, we can assume that planetesimal impacts at speeds of less than 3 times the escape speed v_{esc} are 100% accretionary; 83% of the collisions in our simulations meet this criterion. Furthermore, only for impacts with $v/v_{esc} > 7$—10 do small-body collisions actually become erosive (Okeefe and Ahrens, 1977; Svetsov, 2007). Only 2 out of 3400 collisions in our simulations had $v/v_{esc} > 7$. Thus, our assumption of perfect accretion for planetesimal–embryo impacts probably does not affect our results if planetesimals were indeed km-sized.

The dynamical effects of collisional debris are certainly important, although their effects have barely been explored because of numerical limitations. A continuous source of small bodies after large impacts would likely reduce the eccentricities of the terrestrial planets and make it easy to reproduce the low *AMD* of MVEM (Levison et al., 2005). In addition, planetesimal–planetesimal collisions create collisional cascades that can grind planetesimals to dust, which can then be removed from the system (e.g., Kenyon and Bromley, 2006). However, interactions between the gas disk and small fragments at early times may accelerate embryo growth by stopping collisional cascades and allowing embryos to accrete small fragments (Kenyon and Bromley, 2009).

Tidal damping from small amounts of remnant disk gas can help reduce the eccentricities of the terrestrial planets, as shown by Kominami and Ida (2002, 2004) and Agnor and Ward (2002). Gaseous disks around other stars are thought to disperse in 5 Myr or less (Haisch et al., 2001; Briceño et al., 2001; Pascucci et al., 2006). Such lifetimes correspond to a decrease in gas density to a level of about 10% of the minimum-mass nebular density, while ti-

dal damping can operate down to a level of 10^{-3}–10^{-4}. Nonetheless, for this to be important the gas density must be at least 10^{-4} for the timescale of Earth's accretion, 50–150 Myr (Touboul et al., 2007). For a steady accretion model, the gas density Σ decreases relatively slowly with time t, as $t^{-3/2}$ (Lynden-Bell and Pringle, 1974). Thus, if the Solar Nebula evolved smoothly with a characteristic timescale of 1 Myr, then its density would have decreased to 10% after 5 Myr, but would still be 10^{-3} after 100 Myr. In such a scenario, tidal damping would indeed be an important effect on terrestrial accretion. However, the final phases of disk dissipation are thought to occur after a few Myr (Haisch et al., 2001) on a $\sim 10^5$ year timescale (Simon and Prato, 1995; Wolk and Walter, 1996) and relatively violently, via photo-evaporation (Hollenbach et al., 1994; Johnstone et al., 1998) or potentially the MRI instability (Chiang and Murray-Clay, 2007). Future, more sensitive observations that probe smaller gas densities in disks around young stars will shed light on this issue, but our interpretation of the current state of knowledge is that it is unlikely that tidal damping would dramatically change our results. Indeed, we suspect that the most important source of damping during accretion is likely to be small bodies, i.e., planetesimals and collisional debris.

Secular resonance sweeping during the dispersal of the Solar Nebula could play an important role in terrestrial planet formation if Jupiter and Saturn's orbits have eccentricities of at least $\sim$0.05 (Nagasawa et al., 2005; Thommes et al., 2008). However, if the giant planets' orbits are less eccentric then secular resonances are too weak to have much effect on the outcome (O'Brien et al., 2007). We note that the model of Thommes et al. (2008) invokes this resonant sweeping to induce collisions as well as to shepherd embryos from the asteroid belt inward. However, Thommes et al. assume that the entire inner disk is composed of embryos and do not include any planetesimals in their simulations. Given the strength of aerodynamic gas drag on km-sized bodies (Adachi et al., 1976), planetesimals should also have been shepherded inward by the resonance (e.g., Raymond et al., 2006; Mandell et al., 2007). Indeed, the mass distribution in the area swept out by the secular resonances may have been drastically altered if the resonances were strong enough. We are currently exploring the consequences of this idea.

We did not test an exhaustive number of configurations of Jupiter and Saturn. Indeed, given the relative success of the EEJS configurations, it would be interesting to explore the resonant behavior for other allowed configurations such as, for example, Jupiter and Saturn on their CJS orbits but with eccentricities of 0.1. We plan to search the parameter space of giant planet configurations in future work, focusing on systems with strong mean motion and secular resonances in the inner Solar System.

The majority of this paper has dealt with the effects of the giant planet configuration on the accretion of the inner Solar System. However, we note that the disk's surface density distribution could also play a strong role in the outcome (Raymond et al., 2005). Indeed, we did see changes in the 8 simulations we performed with a flatter, r^{-1} surface density profile. We note that there exists an alternate model that attributes Mars' small mass with the Solar Nebula's density structure (Jin et al., 2008). In Jin et al.'s model the disk is ionized only in certain regions, causing radial variations in the strength of the magneto-rotational instability and therefore in the disk viscosity (Balbus and Hawley, 1991). At the interface between an outer low-viscosity and an inner high-viscosity regime a local dip in the surface density can be created. Jin et al. (2008)'s model has this dip at about Mars' orbital distance. This dip is quite deep but very narrow, although it could have swept over a region of radial with $\sim$1 AU in the lifetime of the disk. When considering accretion in such a disk, it is important to note that the typical planetary feeding zone in our sample has a width of 2–3 AU, much wider than the widest possible gap created in the disk of Jin et al.. Indeed, preliminary simulations using Jin et al.'s disk form Mars analogs that are $\sim 5 M_{Mars}$.

Our simulations are among the highest-resolution to date, but we are still resolution-limited. To accurately model Mars' growth we require that the embryo mass at Mars' orbital distance is smaller than Mars itself, in our case by a factor of 3–6 (Fig. 2). This mass sets the inter-embryo spacing and we are subsequently limited by the number of particles we can integrate in a reasonable time (of several months). Given these restrictions, our simulations may not always adequately model dynamical friction, because the planetesimal-to-embryo mass ratio is relatively small ($\sim$10 at Mars' orbital distance; smaller closer in and larger farther out). Indeed, the EEJS simulations with 2000 planetesimals yielded smaller eccentricities than those with 1000 planetesimals because we could resolve the damping at late times. Our approach contrasts with that of Chambers (2001) and O'Brien et al. (2006), who used fixed-mass embryos and therefore had fixed planetesimal-to-embryo mass ratios of 10 and 40, respectively. The advantage of their approach is that dynamical friction is more consistently modeled, but the disadvantage is that the number of embryos is small and the embryo mass is large, about one Mars mass. Despite the limited resolution and the difficulty with dynamical friction, all of our constraints were met in some simulations, including cases with *AMD* values lower than the MVEM value. We therefore think that our approach is valid, and we anticipate that faster computers will certainly improve the outlook for understanding the origin of the inner Solar System in the coming years.

Acknowledgments

We thank John Chambers and an anonymous second reviewer for comments that helped improve the paper. We also thank John Armstrong for his help in running the bulk of these simulations at Weber State University. We acknowledge useful discussions with Hal Levison, Amara Graps, Michel Dobrijevic, Franck Selsis, Avi Mandell, and Matija Cuk. S.N.R. is grateful for support from NASA Origins of Solar Systems (Grant NNX09AB84G), a NASA Postdoctoral Program fellowship, and to NASA's Astrobiology Institute via the Virtual Planetary Laboratory lead team. D.P.O. acknowledges support from NASA's Planetary Geology and Geophysics and Outer Planets Research programs. This paper is PSI Contribution 460.

References

Abe, Y., Ohtani, E., Okuchi, T., Righter, K., Drake, M. 2000. Water in the early earth. In: Canup, R.M., Righter, K., and 69 collaborating authors (Eds.), Origin of the Earth and Moon. University of Arizona Press, Tucson, pp. 413-433.

Adachi, I., Hayashi, C., Nakazawa, K., 1976. The gas drag effect on the elliptical motion of a solid body in the primordial Solar Nebula. Prog. Theoret. Phys. 56, 1756–1771.

Agnor, C., Asphaug, E., 2004. Accretion efficiency during planetary collisions. Astrophys. J. 613, L157–L160.

Agnor, C.B., Ward, W.R., 2002. Damping of terrestrial-planet eccentricities by density-wave interactions with a remnant gas disk. Astrophys. J. 567, 579–586.

Agnor, C.B., Canup, R.M., Levison, H.F., 1999. On the character and consequences of large impacts in the late stage of terrestrial planet formation. Icarus 142, 219–237.

Alexander, S.G., Agnor, C.B., 1998. N-Body simulations of late stage planetary formation with a simple fragmentation model. Icarus 132, 113–124.

Asphaug, E., Agnor, C.B., Williams, Q., 2006. Hit-and-run planetary collisions. Nature 439, 155–160.

Balbus, S.A., Hawley, J.F., 1991. A powerful local shear instability in weakly magnetized disks. I – Linear analysis. II – Nonlinear evolution. Astrophys. J. 376, 214–233.

Benz, W., 2000. Low velocity collisions and the growth of planetesimals. Space Sci. Rev. 92, 279–294.

Benz, W., Slattery, W.L., Cameron, A.G.W., 1986. The origin of the Moon and the single-impact hypothesis. I. Icarus 66, 515–535.

Benz, W., Slattery, W.L., Cameron, A.G.W., 1988. Collisional stripping of Mercury's mantle. Icarus 74, 516–528.

Boss, A.P., 1998. Temperatures in protoplanetary disks. Annu. Rev. Earth and Pl. Sc. 26, 53–80.
Brasser, R., Duncan, M.J., Levison, H.F., 2006. Embedded star clusters and the formation of the Oort cloud. Icarus 184, 59–82.
Briceño, C. and 10 colleagues, 2001. The CIDA-QUEST large-scale survey of orion OB1: Evidence for rapid disk dissipation in a dispersed stellar population. Science 291, 93–97.
Brown, M.E., Trujillo, C., Rabinowitz, D., 2004. Discovery of a candidate inner Oort cloud planetoid. Astrophys. J. 617, 645–649.
Canup, R.M., 2004. Simulations of a late lunar-forming impact. Icarus 168, 433–456.
Canup, R.M., 2008. Lunar-forming collisions with pre-impact rotation. Icarus 196, 518–538.
Canup, R.M., Asphaug, E., 2001. Origin of the Moon in a giant impact near the end of the Earth's formation. Nature 412, 708–712.
Canup, R.M., Pierazzo, E., 2006. Retention of water during planet-scale collisions. In: Proc. of the 37th Annual Lunar and Planetary Science Conference, vol. 37, p. 2146.
Capobianco, C.C., Duncan, M.J., Levison, H.F., 2008. Planet migration in planetesimal disks: Effects of a gas disk. In: Proc. of the AAS/Division of Dynamical Astronomy Meeting, vol. 39, p. #03.04.
Chambers, J.E., 1999. A hybrid symplectic integrator that permits close encounters between massive bodies. Mon. Not. R. Astron. Soc. 304, 793–799.
Chambers, J.E., 2001. Making More Terrestrial Planets. Icarus 152, 205–224.
Chambers, J.E., 2004. Planetary accretion in the inner Solar System. Earth Planet. Sci. Lett. 223, 241–252.
Chambers, J.E., 2007. On the stability of a planet between Mars and the asteroid belt: Implications for the Planet V hypothesis. Icarus 189, 386–400.
Chambers, J.E., Cassen, P., 2002. The effects of Nebula surface density profile and giant-planet eccentricities on planetary accretion in the inner Solar System. Meteorit. Planet. Sci. 37, 1523–1540.
Chambers, J.E., Wetherill, G.W., 1998. Making the terrestrial planets: N-Body integrations of planetary embryos in three dimensions. Icarus 136, 304–327.
Chambers, J.E., Wetherill, G.W., 2001. Planets in the asteroid belt. Meteorit. Planet. Sci. 36, 381–399.
Chiang, E., Murray-Clay, R., 2007. Inside-out evacuation of transitional protoplanetary discs by the magneto-rotational instability. Nature Physics 3, 604–608.
Chiang, E., Lithwick, Y., Murray-Clay, R., Buie, M., Grundy, W., Holman, M., 2007. A brief history of transneptunian space. Protostars Planets V, 895–911.
Cresswell, P., Dirksen, G., Kley, W., Nelson, R.P., 2007. On the evolution of eccentric and inclined protoplanets embedded in protoplanetary disks. Astron. Astrophys. 473, 329–342.
Cuzzi, J.N., Hogan, R.C., Shariff, K., 2008. Toward planetesimals: Dense chondrule clumps in the protoplanetary Nebula. Astrophys. J. 687, 1432–1447.
D'Angelo, G., Lubow, S.H., Bate, M.R., 2006. Evolution of giant planets in eccentric disks. Astrophys. J. 652, 1698–1714.
Delsemme, A.H., 1992. Cometary origin of carbon, nitrogen, and water on the Earth. Origins Life Evol. Biosphere 21, 279–298.
Dullemond, C.P., Dominik, C., 2004. The effect of dust settling on the appearance of protoplanetary disks. Astron. Astrophys. 421, 1075–1086.
Duncan, M., Quinn, T., Tremaine, S., 1987. The formation and extent of the Solar System comet cloud. Astron. J. 94, 1330–1338.
Eisner, J.A., 2007. Water vapour and hydrogen in the terrestrial-planet-forming region of a protoplanetary disk. Nature 447, 562–564.
Eisner, J.A., Hillenbrand, L.A., White, R.J., Akeson, R.L., Sargent, A.I., 2005. Observations of T Tauri disks at sub-AU radii: Implications for magnetospheric accretion and planet formation. Astrophys. J. 623, 952–966.
Fernandez, J.A., Ip, W.-H., 1984. Some dynamical aspects of the accretion of Uranus and Neptune – The exchange of orbital angular momentum with planetesimals. Icarus 58, 109–120.
Ford, E.B., Chiang, E.I., 2007. The formation of ice giants in a packed oligarchy: Instability and aftermath. Astrophys. J. 661, 602–615.
Genda, H., Abe, Y., 2005. Enhanced atmospheric loss on protoplanets at the giant impact phase in the presence of oceans. Nature 433, 842–844.
Goldreich, P., Sari, R., 2003. Eccentricity evolution for planets in gaseous disks. Astrophys. J. 585, 1024–1037.
Goldreich, P., Ward, W.R., 1973. The formation of planetesimals. Astrophys. J. 183, 1051–1062.
Gomes, R.S., 2003. The origin of the Kuiper Belt high-inclination population. Icarus 161, 404–418.
Gomes, R.S., Morbidelli, A., Levison, H.F., 2004. Planetary migration in a planetesimal disk: Why did Neptune stop at 30 AU? Icarus 170, 492–507.
Gomes, R., Levison, H.F., Tsiganis, K., Morbidelli, A., 2005. Origin of the cataclysmic late heavy bombardment period of the terrestrial planets. Nature 435, 466–469.
Gradie, J., Tedesco, E., 1982. Compositional structure of the asteroid belt. Science 216, 1405–1407.
Greenberg, R., Hartmann, W.K., Chapman, C.R., Wacker, J.F., 1978. Planetesimals to planets – Numerical simulation of collisional evolution. Icarus 35, 1–26.
Grimm, R.E., McSween, H.Y., 1993. Heliocentric zoning of the asteroid belt by aluminum-26 heating. Science 259, 653–655.
Hahn, J.M., Malhotra, R., 1999. Orbital evolution of planets embedded in a planetesimal disk. Astron. J. 117, 3041–3053.
Haisch Jr., K.E., Lada, E.A., Lada, C.J., 2001. Disk frequencies and lifetimes in young clusters. Astrophys. J. 553, L153–L156.
Halliday, A.N., 2004. Mixing, volatile loss and compositional change during impact-driven accretion of the Earth. Nature 427, 505–509.
Hayashi, C. 1981. Structure of the solar nebula, growth and decay of magnetic fields and effects of magnetic and turbulent viscosities on the nebula. Prog. Theor. Phys. Supp. 70, 35-53.
Heppenheimer, T.A., 1980. Secular resonances and the origin of eccentricities of Mars and the asteroids. Icarus 41, 76–88.
Hollenbach, D., Johnstone, D., Lizano, S., Shu, F., 1994. Photoevaporation of disks around massive stars and application to ultracompact H II regions. Astrophys. J. 428, 654–669.
Ida, S., Makino, J., 1992. N-body simulation of gravitational interaction between planetesimals and a protoplanet. II – Dynamical friction. Icarus 98, 28–37.
Ida, S., Makino, J., 1993. Scattering of planetesimals by a protoplanet – Slowing down of runaway growth. Icarus 106, 210.
Ikoma, M., Genda, H., 2006. Constraints on the mass of a habitable planet with water of nebular origin. Astrophys. J. 648, 696–706.
Jin, L., Arnett, W.D., Sui, N., Wang, X., 2008. An interpretation of the anomalously low mass of Mars. Astrophys. J. 674, L105–L108.
Johansen, A., Oishi, J.S., Low, M.-M.M., Klahr, H., Henning, T., Youdin, A., 2007. Rapid planetesimal formation in turbulent circumstellar disks. Nature 448, 1022–1025.
Johnstone, D., Hollenbach, D., Bally, J., 1998. Photoevaporation of disks and clumps by nearby massive stars: Application to disk destruction in the orion Nebula. Astrophys. J. 499, 758.
Kaib, N.A., Quinn, T., 2008. The formation of the Oort cloud in open cluster environments. Icarus 197, 221–238.
Kasting, J.F., 1988. Runaway and moist greenhouse atmospheres and the evolution of Earth and Venus. Icarus 74, 472–494.
Kenyon, S.J., Bromley, B.C., 2006. Terrestrial planet formation. I. The transition from oligarchic growth to chaotic growth. Astron. J. 131, 1837–1850.
Kenyon, S.J., Bromley, B.C., 2009. Rapid formation of icy super-Earths and the cores of gas giant planets. Astrophys. J. 690, L140–L143.
Kerridge, J.F., 1985. Carbon, hydrogen and nitrogen in carbonaceous chondrites: Abundances and isotopic compositions in bulk samples. Geochim. Cosmochim. Acta 49, 1707–1714.
Kleine, T., Münker, C., Mezger, K., Palme, H., 2002. Rapid accretion and early core formation on asteroids and the terrestrial planets from Hf-W chronometry. Nature 418, 952–955.
Kley, W., Dirksen, G., 2006. Disk eccentricity and embedded planets. Astron. Astrophys. 447, 369–377.
Kokubo, E., Ida, S., 1998. Oligarchic growth of protoplanets. Icarus 131, 171–178.
Kokubo, E., Ida, S., 2000. Formation of protoplanets from planetesimals in the solar nebula. Icarus 143, 15–27.
Kokubo, E., Ida, S., 2002. Formation of protoplanet systems and diversity of planetary systems. Astrophys. J. 581, 666–680.
Kominami, J., Ida, S., 2002. The effect of tidal interaction with a gas disk on formation of terrestrial planets. Icarus 157, 43–56.
Kominami, J., Ida, S., 2004. Formation of terrestrial planets in a dissipating gas disk with Jupiter and Saturn. Icarus 167, 231–243.
Lamers, H.J.G.L.M., Gieles, M., Bastian, N., Baumgardt, H., Kharchenko, N.V., Portegies Zwart, S., 2005. An analytical description of the disruption of star clusters in tidal fields with an application to Galactic open clusters. Astron. Astrophys. 441, 117–129.
Laskar, J., 1997. Large scale chaos and the spacing of the inner planets. Astron. Astrophys. 317, L75–L78.
Lecar, M., Franklin, F., 1997. The solar nebula, secular resonances, gas drag, and the Asteroid Belt. Icarus 129, 134–146.
Lécuyer, C., Gillet, P., Robert, F., 1998. The hydrogen isotope composition of sea water and the global water cycle. Chem. Geol. 145, 249–261.
Levison, H.F., Agnor, C., 2003. The role of giant planets in terrestrial planet formation. Astron. J. 125, 2692–2713.
Levison, H.F., Morbidelli, A., 2003. The formation of the Kuiper belt by the outward transport of bodies during Neptune's migration. Nature 426, 419–421.
Levison, H.F., Morbidelli, A., 2007. Models of the collisional damping scenario for icegiant planets and Kuiper belt formation. Icarus 189, 196–212.
Levison, H., Nesvorny, D., Agnor, C., Morbidelli, A., 2005. The role of dynamical friction in terrestrial planet formation. Bull. Am. Astron. Soc. 37, 666.
Lynden-Bell, D., Pringle, J.E., 1974. The evolution of viscous discs and the origin of the nebular variables. Mon. Not. R. Astron. Soc. 168, 603–637.
Malhotra, R., 1993. The origin of Pluto's peculiar orbit. Nature 365, 819.
Malhotra, R., 1995. The origin of Pluto's orbit: Implications for the Solar System beyond Neptune. Astron. J. 110, 420.
Mandell, A.M., Raymond, S.N., Sigurdsson, S., 2007. Formation of Earth-like planets during and after giant planet migration. Astrophys. J. 660, 823–844.
Matsui, T., Abe, Y., 1986. Evolution of an impact-induced atmosphere and magma ocean on the accreting earth. Nature 319, 303–305.
Melosh, H.J., 1984. Impact ejection, spallation, and the origin of meteorites. Icarus 59, 234–260.
Millan-Gabet, R., Malbet, F., Akeson, R., Leinert, C., Monnier, J., Waters, R., 2007. The circumstellar environments of young stars at AU scales. Protostars Planets V, 539–554.
Minton, D.A., Malhotra, R., 2009. A record of planet migration in the main asteroid belt. Nature 457, 1109–1111.
Morbidelli, A., Chambers, J., Lunine, J.I., Petit, J.M., Robert, F., Valsecchi, G.B., Cyr, K.E., 2000. Source regions and time scales for the delivery of water to Earth. Meteorit. Planet. Sci. 35, 1309–1320.

Morbidelli, A., Petit, J.-M., Gladman, B., Chambers, J., 2001. A plausible cause of the late heavy bombardment. Meteorit. Planet. Sci. 36, 371–380.
Morbidelli, A., Levison, H.F., Tsiganis, K., Gomes, R., 2005. Chaotic capture of Jupiter's Trojan asteroids in the early Solar System. Nature 435, 462–465.
Morbidelli, A., Tsiganis, K., Crida, A., Levison, H.F., Gomes, R., 2007. Dynamics of the giant planets of the Solar System in the gaseous protoplanetary disk and their relationship to the current orbital architecture. Astron. J. 134, 1790–1798.
Morishima, R., Schmidt, M.W., Stadel, J., Moore, B., 2008. Formation and accretion history of terrestrial planets from runaway growth through to late time: Implications for orbital eccentricity. Astrophys. J. 685, 1247–1261.
Muralidharan, K., Deymier, P., Stimpfl, M., de Leeuw, N.H., Drake, M.J., 2008. Origin of water in the inner Solar System: A kinetic Monte Carlo study of water adsorption on forsterite. Icarus 198, 400–407.
Nagasawa, M., Tanaka, H., Ida, S., 2000. Orbital evolution of asteroids during depletion of the Solar Nebula. Astron. J. 119, 1480–1497.
Nagasawa, M., Lin, D.N.C., Thommes, E., 2005. Dynamical shake-up of planetary systems I. Embryo trapping and induced collisions by the sweeping secular resonance and embryo-disk tidal interaction. Astrophys. J. 635, 578–598.
Nagasawa, M., Thommes, E.W., Kenyon, S.J., Bromley, B.C., Lin, D.N.C., 2007. The diverse origins of terrestrial-planet systems. Protostars Planets V, 639–654.
Nimmo, F., Agnor, C.B., 2006. Isotopic outcomes of N-body accretion simulations: Constraints on equilibration processes during large impacts from Hf/W observations. Earth Planet. Sci. Lett. 243, 26–43.
Nimmo, F., Kleine, T., 2007. How rapidly did Mars accrete? Uncertainties in the Hf W timing of core formation. Icarus 191, 497–504.
O'Brien, D.P., Morbidelli, A., Levison, H.F., 2006. Terrestrial planet formation with strong dynamical friction. Icarus 184, 39–58.
O'Brien, D.P., Morbidelli, A., Bottke, W.F., 2007. The primordial excitation and clearing of the asteroid belt–Revisited. Icarus 191, 434–452.
Okeefe, J.D., Ahrens, T.J., 1977. Meteorite impact ejecta – Dependence of mass and energy lost on planetary escape velocity. Science 198, 1249–1251.
Owen, T., Bar-Nun, A., 1995. Comets, impacts and atmospheres. Icarus 116, 215–226.
Papaloizou, J.C.B., Nelson, R.P., Masset, F., 2001. Orbital eccentricity growth through disc-companion tidal interaction. Astron. Astrophys. 366, 263–275.
Pascucci, I., and 19 colleagues, 2006. Formation and evolution of planetary systems: Upper limits to the gas mass in disks around Sun-like stars. Astrophys. J. 651, 1177–1193.
Petit, J.-M., Morbidelli, A., Chambers, J., 2001. The primordial excitation and clearing of the asteroid belt. Icarus 153, 338–347.
Pollack, J.B., Hubickyj, O., Bodenheimer, P., Lissauer, J.J., Podolak, M., Greenzweig, Y., 1996. Formation of the giant planets by concurrent accretion of solids and gas. Icarus 124, 62–85.
Quinn, T.R., Tremaine, S., Duncan, M., 1991. A three million year integration of the Earth's orbit. Astron. J. 101, 2287–2305.
Rauch, K.P., Holman, M., 1999. Dynamical chaos in the Wisdom–Holman integrator: Origins and solutions. Astron. J. 117, 1087–1102.
Raymond, S.N., 2006. The search for other Earths: Limits on the giant planet orbits that allow habitable terrestrial planets to form. Astrophys. J. 643, L131–L134.
Raymond, S.N., 2008. Terrestrial planet formation in extra-solar planetary systems. In: Proc of the IAU Symposium, vol. 249, pp. 233–250.
Raymond, S.N., Quinn, T., Lunine, J.I., 2004. Making other earths: Dynamical simulations of terrestrial planet formation and water delivery. Icarus 168, 1–17.
Raymond, S.N., Quinn, T., Lunine, J.I., 2005. Terrestrial planet formation in disks with varying surface density profiles. Astrophys. J. 632, 670–676.
Raymond, S.N., Mandell, A.M., Sigurdsson, S., 2006. Exotic Earths: Forming habitable worlds with giant planet migration. Science 313, 1413–1416.
Raymond, S.N., Quinn, T., Lunine, J.I., 2006. High-resolution simulations of the final assembly of Earth-like planets I. Terrestrial accretion and dynamics. Icarus 183, 265–282.
Raymond, S.N., Quinn, T., Lunine, J.I., 2007. High-resolution simulations of the final assembly of Earth-like planets. 2. Water delivery and planetary habitability. Astrobiology 7, 66–84.
Robert, F., Epstein, S., 1982. The concentration and isotopic composition of hydrogen, carbon and nitrogen in carbonaceous meteorites. Geochim. Cosmochim. Acta 46, 81–95.
Safronov, V.S., 1969. Evoliutsiia doplanetnogo oblaka, 1969.
Simon, M., Prato, L., 1995. Disk dissipation in single and binary young star systems in Taurus. Astrophys. J. 450, 824.
Strom, R.G., Malhotra, R., Ito, T., Yoshida, F., Kring, D.A., 2005. The origin of planetary impactors in the inner Solar System. Science 309, 1847–1850.
Svetsov, V.V., 2007. Atmospheric erosion and replenishment induced by impacts of cosmic bodies upon the Earth and Mars. Solar System Res. 41, 28–41.
Tera, F., Papanastassiou, D.A., Wasserburg, G.J., 1974. Isotopic evidence for a terminal lunar cataclysm. Earth Planet Sci. Lett. 22, 1.
Thommes, E., Nagasawa, M., Lin, D.N.C., 2008. Dynamical shake-up of planetary systems. II. N-Body simulations of Solar System terrestrial planet formation induced by secular resonance sweeping. Astrophys. J. 676, 728–739.
Touboul, M., Kleine, T., Bourdon, B., Palme, H., Wieler, R., 2007. Late formation and prolonged differentiation of the Moon inferred from W isotopes in lunar metals. Nature 450, 1206–1209.
Tsiganis, K., Gomes, R., Morbidelli, A., Levison, H.F., 2005. Origin of the orbital architecture of the giant planets of the Solar System. Nature 435, 459–461.
Ward, W.R., 1981. Solar nebula dispersal and the stability of the planetary system. I – Scanning secular resonance theory. Icarus 47, 234–264.
Ward, W.R., 1993. Density waves in the Solar Nebula – Planetesimal velocities. Icarus 106, 274.
Weidenschilling, S.J., 1977a. The distribution of mass in the planetary system and solar nebula. Astrophys. Space Sci. 51, 153–158.
Weidenschilling, S.J., 1977b. Aerodynamics of solid bodies in the Solar Nebula. Mon. Not. R. Astron. Soc. 180, 57–70.
Weidenschilling, S.J., 1978. Iron/silicate fractionation and the origin of Mercury. Icarus 35, 99–111.
Weidenschilling, S.J., 1980. Dust to planetesimals – Settling and coagulation in the Solar Nebula. Icarus 44, 172–189.
Weidenschilling, S.J., Cuzzi, J.N., 1993. Formation of planetesimals in the Solar Nebula. Protostars Planets III, 1031–1060.
Weidenschilling, S.J., Spaute, D., Davis, D.R., Marzari, F., Ohtsuki, K., 1997. Accretional evolution of a planetesimal swarm. Icarus 128, 429–455.
Wetherill, G.W., 1985. Occurrence of giant impacts during the growth of the terrestrial planets. Science 228, 877–879.
Wetherill, G.W., 1991. Why isn't Mars as big as Earth? Lunar Planet. Inst. Sci. Conf. Abstr. 22, 1495.
Wetherill, G.W., 1992. An alternative model for the formation of the asteroids. Icarus 100, 307–325.
Wetherill, G.W., 1996. The formation and habitability of extra-solar planets. Icarus 119, 219–238.
Wetherill, G.W., Stewart, G.R., 1993. Formation of planetary embryos – Effects of fragmentation, low relative velocity, and independent variation of eccentricity and inclination. Icarus 106, 190–209.
Wolk, S.J., Walter, F.M., 1996. A search for protoplanetary disks around naked T Tauri stars. Astron. J. 111, 2066.
Yin, Q., Jacobsen, S.B., Yamashita, K., Blichert-Toft, J., Télouk, P., Albarède, F., 2002. A short timescale for terrestrial planet formation from Hf-W chronometry of meteorites. Nature 418, 949–952.
Youdin, A.N., Shu, F.H., 2002. Planetesimal formation by gravitational instability. Astrophys. J. 580, 494–505.